# Tropical Tropospheric Ozone Trends (1998 to 2023): New Perspectives from SHADOZ, IAGOS and OMI/MLS Observations *Accepted Version -20 Aug 2025*

**Anne M. Thompson[1,2]\*, Ryan M. Stauffer[1], Debra E. Kollonige[1,3], Jerald R. Ziemke[1,4], Bryan J. Johnson[5], Gary A. Morris[5], Patrick Cullis[5], María Cazorla[6], Jorge Andres Diaz[7], Ankie Piters[8], Igor Nedeljkovic[8], Truus Warsodikromo[9], Francisco Raimundo Silva[10], E. Thomas Northam[11], Patrick Benjamin[12], Thumeka Mkololo[13], Tshidi Machinini[13], Christian Félix[14], Gonzague Romanens[14], Syprose Nyadida[15], Jérôme Brioude[16], Stéphanie Evan[16], Jean-Marc Metzger[17], Ambun Dindang[18], Yuzaimi B Mahat[18], Mohan Kumar Sammathuria[18], Norazura Binti Zakaria[1], Ninong Komala[19], Shin-Ya Ogino[20], Nguyen Thi Quyen[21], Francis S. Mani[22], Miriama Vuiyasawa[22], David Nardini[23], Matthew Martinsen[24], Darryl T. Kuniyuki[5], Katrin Müller[25], Audrey Gaudel[24], Pawel Wolff[26], Bastien Sauvage[27]**

\*Corresponding author: Anne M. Thompson (anne.m.thompson@nasa.gov)

[1]NASA/Goddard Space Flight Center (GSFC), Greenbelt, MD, USA anne.m.thompson@nasa.gov; ORCID: 0000-0002-7829-0920; ryan.m.stauffer@nasa.gov; ORCID: 0000-0002-8583-7795
[2]University of Maryland-Baltimore County, Baltimore, MD 21228
[3]Science Systems and Applications, Inc., Lanham, MD, debra.e.kollonige@nasa.gov; ORCID: 0000-0002-6597-328X;
[4]Morgan State Univ., Baltimore, MD, jerald.r.ziemke@nasa.gov; ORCID: 0000-0002-5575-3654; [5]NOAA/Global Monitoring Lab, Boulder, CO; bryan.johnson2425@gmail.com; gary.morris@noaa.gov ORCID: 0000-0002-2196-8454; patrick.cullis@noaa.gov ORCID: 0000-0002-8723-6280; darryl.t.kuniyuki@noaa.gov; audrey.gaudel@noaa.gov ORCID: https://orcid.org/0000-0003-2727-213X
[6]Universidad San Francisco de Quito USFQ, Colegio de Ciencias e Ingenierías, Instituto de Investigaciones Atmosféricas, Quito, Ecuador; mcazorla@usfq.edu.ec; https://orcid.org/0000-0001-5295-2968
[7] Universidad de Costa Rica, San Jose, Costa Rica, jorge.andres.diaz@gmail.com
[8]Royal Netherlands Meteorological Institute (KNMI), De Bilt, The Netherlands, ankie.piters@knmi.nl, 0000-0002-8234-1022; igor.nedeljkovic@knmi.nl
[9]Meteorological Service of Surinam, Paramaribo, Surinam, wtruus98@gmail.com
[10] Brazilian National Institute of Space Research (INPE), Natal, Brazil, fraimundo.raimundo@inpe.br
[11] Science Systems and Applications, Inc., Wallops Island, VA., USA, e.thomas.northam@nasa.gov
[12] US Space Force Base, Patrick, FSB, FL, USA, Yang Enterprises, Inc., patrick.benjamin.1.ctr.gb@spaceforce.mil
[13] South African Weather Service (SAWS), Pretoria, South Africa, thumeka.mkololo@weathersa.co.za, tshidi.machinini@weathersa.co.za
[14] MeteoSwiss, Payerne, Switzerland, christian.felix@meteoswiss.ch, gonzague.romanens@meteoswiss.ch
[15] Kenya Meteorological Department, Nairobi, Kenya, syprosenyadida1@gmail.com

[16] Laboratoire de l'Atmosphère et des Cyclones (LACy), UMR 8105 CNRS, Université de La Réunion, Météo-France, Saint-Denis, France, jerome.brioude@univ-reunion.fr 0000-0002-5603-7924; stephanie.evan@univ-reunion.fr, 0000-0003-1014-0907
[17] Observatoire des Sciences de l'Univers de La Réunion (OSU-Réunion), UAR 3365, Université de La Réunion, CNRS, Météo France, IRD, Saint-Denis, France jean-marc.metzger@univ-reunion.fr
[18] Malaysian Meteorological Department, Petaling Jaya, Malaysia, ambun@met.gov.my, yuzaimi@met.gov.my, mohan@met.gov.my, norazura@met.gov.my
[19] National Research and Innovation Agency (BRIN), Bandung, Indonesia, ninongk@yahoo.com; ORCID: 0000-0003-3869-9622
[20] Japan Agency for Marine-Earth Science and Technology (JAMSTEC), Research Institute for Global Change, Yokosuka, Japan, ogino-sy@jamstec.go.jp ORCID: 0000-0001-9167-4833
[21] Aero-Meteorological Observatory (AMO), Viet Nam Meteorological and Hydrological Administration, quyenck@gmail.com
[22] The University of the South Pacific (USP), Suva, Fiji, francis.mani@usp.ac.fj, 0000-0001-6596-644x miriamavuiyasawa@gmail.com
[23] CIMAR, Univ. Hawaii at Manoa, Honolulu, HI; david.nardini@noaa.gov
[24] CIRES, Univ. Colorado, Boulder, CO, matthew.martinsen@noaa.gov

53    [25] Alfred - Wegener – Institut, Helmholtz Centre for Polar and Marine Research, Potsdam, Germany,
54    katrin.mueller@awi.de; ORCID: 0000-0002-6891-6889
55    [26] SEDOO, Univ. Paul Sabatier III, Toulouse, France; now at ECMWF, Bonn, Germany, pawel.wolff@ecmwf.int;
56    ORCID: 0000-0002-2082-6825
57    [27] Laboratoire d'Aérologie Observatoire Midi-Pyrénées, 14 av. E. Belin, 31400 Toulouse France;
58    Bastien.sauvage@univ-tlse3.fr; ORCID : 0000-0003-3410-2139
59

62    **Abstract.** Tropospheric ozone trends are important indicators of climate forcing and surface pollution
63    yet relevant satellite observations are too uncertain for assessments. The assessment project TOAR-II
64    has used multi-instrument, ground-based data for global trends over 2000-2022 (Van Malderen et al.,
65    2025a,b). For the tropics trends are derived from SHADOZ ozonesonde profiles (Thompson et al., 2021,
66    "T21"; Stauffer et al., 2024) or combinations of satellite, SHADOZ and IAGOS aircraft measurements
67    (Gaudel et al., 2024). We extend T21 that covered 1998-2019, analyzing SHADOZ data at 5 sites with a
68    Multiple Linear Regression (MLR) model for 1998-2023, and reporting trends for two free tropospheric
69    (FT) segments, lowermost stratosphere and total tropospheric column ($TrCO_{sonde}$). Trends for the Aura
70    period, 2005-2023, are computed from OMI/MLS $TrCO_{satellite}$. We find: (1) Extending SHADOZ analyses
71    four years shows little change from T21; $TrCO_{sonde}$ trends are small (0.5-1 DU/dec) except over SE Asia.
72    (2) Annual trends for $TrCO_{sonde}$ and OMI/MLS $TrCO_{satellite}$ agree within uncertainties with largest
73    differences at Samoa. Sensitivity tests show: (1) adding thousands of FT IAGOS profiles to SHADOZ
74    yields little change in trends; SHADOZ sampling is sufficient. (2) QR and MLR median trends are both
75    near-zero but QR captures extremes (5%-ile, 95-%ile) with changes up to $\pm1$ DU/decade (p < 0.10). (3)
76    Twelve-year analyses for trends lead to uncertainty changes too large for an assessment. This study and
77    Van Malderen et al. (2025a;b) provide the most reliable TOAR-II trends to date: over the past ~25 years,
78    tropical FT ozone changes are modest, ~(-3-+3)%/decade, except over SE Asia.
79

80    **1 Introduction**

81        The importance of tropical tropospheric ozone in atmospheric composition and climate variability

82    has long been known (Lacis et al., 1990; Schwartzkopf and Ramaswamy, 1993). Although the thickness

83    of total column ozone (TCO) in the tropics (~250-325 Dobson Units, DU; 1 DU=$2.69 \times 10^{16} cm^{-2}$) is much

84    less than in the extra-tropics (350-450 DU), the latitude band from -30° to +30° covers roughly 1/2 of

85    the Earth's surface. The tropical tropospheric column (TrCO) varies from ~15-20 DU over the Pacific to

86    50-60 DU over the Atlantic, giving rise to a distinctive wave-one pattern in both TCO and TrCO

87    (Thompson et al., 2003). Tropical tropospheric ozone is a major source of global OH (hydroxyl radical),

88    key to Earth's oxidizing capacity (Thompson et al., 1992), controlling the lifetimes of countless biogenic

89    and anthropogenic species. Global OH also controls the lifetime of methane, a powerful greenhouse gas

90    with both natural and anthropogenic sources (Khalil, 2000). Methane ($CH_4$) increases alone add ozone

91    to the troposphere and methane's oxidation by OH to carbon monoxide (CO), that also affects the

92    amount of OH, establishes a feedback cycle among $O_3$-OH-$CH_4$-CO (Thompson and Cicerone, 1986;

93    Thompson et al., 1990). Regional variability in factors controlling the cycle derives from local levels of

94    the shorter-lived nitrogen oxides and reactive volatile organic compounds. The tropics/subtropics (-30°

95  to +30°) is where the "tropical pipe" (Plumb, 1996) carries ozone and ozone-destroying trace species

96  from the tropics into the mid-latitude lowermost stratosphere (LMS).

97    Trends in tropical tropospheric and LMS ozone are of interest for several reasons. First, free

98  tropospheric (FT) ozone is an important greenhouse gas. There is a potential for significant changes in

99  FT ozone because parts of the tropics are in areas of rapid changes in emissions. These may be caused

100  by economic development (Zhang et al., 2016) and/or variations in land-use and fire activity

101  (Christensen et al., 2022; Tsivlidou et al., 2023). Second, with relatively low ozone amounts relative to

102  the extra-tropics, ozone near the tropical tropopause is highly sensitive to dynamical interactions

103  Randel et al. (2007). Analyses of ozone profiles over the past ~25 years have found regional

104  meteorological changes propagating to seasonal ozone increases. Stauffer et al. (2024) verified that a

105  suspected decline in early-year convection (Thompson et al., 2021; hereafter T21) drove 1998-2022

106  ozone increases over equatorial southeast Asia. New reports on decreasing tropical cloud cover

107  (Tselioudis et al., 2025) and a shift in ITCZ location (Aumann et al., 2024) may indicate changes in

108  convection. At Réunion Island shifting anticyclones caused an increase in FT ozone from 1998-2023

109  (Millet et al., 2025). Recurring influences of climate oscillations, i.e., the Quasi-biennial Oscillation, ENSO,

110  Indian Ocean Dipole,  on FT and LMS ozone are well-documented in ozonesonde and satellite data

111  (Thompson et al., 2001; Ziemke et al., 2003; Ziemke et al., 2006; Ziemke et al., 2019; Lee et al., 2010;

112  Randel and Thompson, 2011; Thompson et al., 2011).

113

114    1.1    **The TOAR Project.  Challenges in Assessing Tropospheric Ozone Trends**

115    Context for this study comes from the International Global Atmospheric Chemistry/Tropospheric

116  Ozone Assessment Report (IGAC/TOAR) that is completing its second phase, TOAR II, initiated in 2020.

117  The first TOAR, designated here as TOAR I and published as a collection of 11 papers in *Elementa*, 2017-

118  2020; https://online.ucpress.edu/elementa/toar) included an assessment of surface ozone changes

119  (Chang et al., 2017) based on a vast set of surface ozone measurements from 7 continents (Schultz et al.,

120  2017). The TOAR I papers concluded that a comprehensive assessment of tropospheric ozone trends

121  based on observations is very challenging. For example, because the FT is the region of greatest

122  radiative forcing by ozone, the trends community needs profile data. A TOAR I evaluation by Tarasick et

123  al. (2019) pointed out the uneven geographic coverage of ozone profiles from soundings (~60 publicly

124  available station records since the early 1990s) and aircraft landing and takeoff profiles to ~250 hPa

125  that are used for FT ozone analyses. Tarasick et al. (2019) also questioned the suitability of all ground-

126  based (sonde, aircraft, lidar, passive spectrometers) for monitoring FT ozone using illustrations from

127  multi-decadal records that include obsolete techniques, evolving versions of instruments and/or

128  inconsistent absolute calibration. Nonetheless, several follow-on studies to TOAR I employed sonde

129  (T21) and commercial aircraft data (from the In-service Aircraft for a Global Observing System, IAGOS;

3

130　https://iagos.org), with 5-10% accuracy or better, to estimate trends from the 1990s to ~2018 (Gaudel

131　et al., 2020; Thouret et al., 2022).

132　　Efforts in TOAR I to fill gaps with tropospheric ozone estimates from satellite data, preferred over in-

133　situ methods for their even global coverage, were mixed. Gaudel et al. (2018) pointed out that trends

134　derived from five satellite products covering tropics and mid-latitudes for the 2005-2016 period

135　differed from one another not only in magnitude but in sign. The newer TOAR II evaluation of six

136　satellite products for 2015-2019 over the tropics (Gaudel et al., 2024), where satellite estimates tend to

137　be most reliable (T21), exhibited a range of values. Not only were uncertainties among the products

138　highly variable; comparisons of monthly mean satellite columns with sonde and IAGOS profiles up to

139　270 hPa exhibited $r^2$ correlations as low as 0.27.

140　　Other TOAR II studies also reveal a persistent uncertainty in the application of satellite data for

141　trends analyses. Pope et al. (2023) published global trends from 2005-2017 OMI (Ozone Monitoring

142　Instrument on board the NASA Aura satellite) TCO data that are too high because of a drift in OMI that

143　was corrected in Gaudel et al. (2024). The latter study led to a satellite-based estimate for tropical ozone

144　trends for 2005-2019 of ~(0.5-3) ppbv/decade for TrCO, similar or slightly larger than T21. Trends

145　determined from non-UV satellite instruments have been disappointing (Gaudel et al., 2018). A TOAR II

146　contribution by Froidevaux et al. (2025) examined changes in tropical ozone (±26 deg latitude) over the

147　2005 to 2020 period using measurements from the three lowest levels of MLS (Microwave Limb

148　Sounder on board Aura). Unfortunately, the zonal structure of MLS data at the 146 hPa and 213 hPa

149　levels (Fig. 1 in Froidevaux et al., 2025) shows that the prominent ozone wave-one feature, associated

150　with the Walker circulation (Thompson et al., 2003; Thompson et al., 2017), is absent, i.e., MLS does not

151　capture regional differences as OMI-based products do. Froidevaux et al. (2025; Figs. 1, 2, 5) compare

152　the MLS global structure to ozone output at 215 and 146 hPa from 3 models, Whole Atmosphere

153　Community Climate Model (WACCM6) and two variants of the Community Atmosphere Model with

154　Chemistry (CAM-Chem), each variant using different anthropogenic emissions. The models are likewise

155　zonally uniform in upper tropospheric ozone so they do not yield meaningful tropical upper

156　tropospheric ozone trends either.

157　　A TOAR II-related investigation (Boynard et al., 2025) uses IR-based retrievals from the MetOP IASI

158　(Infrared Atmospheric Sounding Interferometer)  satellite instrument to determine trends for the

159　period 2008-2023. As in Gaudel et al. (2018) the newer IASI tropospheric ozone climatology differs from

160　that of UV-based products; IASI's negative ozone trends also disagree with increases from UV-based

161　products. Boynard et al. (2025) offer little explanation for the discrepancies. They note that their 12-yr

162　period trends (2008-2019), roughly half as long as the sonde or aircraft trends in T21 or Gaudel et al.

163　(2024), may be too short for a statistically robust result. Pennington et al. (2025) does provide some

insight into long-term changes of 3 satellite IR products (TROPESS CrIS, AIRS, AIRS+OMI) compared to ozonesondes and finds that the global tropospheric ozone satellite-sonde bias is approximately one third the magnitude of trends in global tropospheric ozone reported by TOAR I.

Keppens et al. (2025) addressed the question of whether satellite data harmonization for nadir ozone profile and column products improves satellite data consistency for both their mean distributions and long-term changes. They concluded that their harmonization methods reduce inter-product dispersion by about 10% when comparing to global ozonesonde datasets from 43 sites, but there is a significant meridional dependence, and the dispersion reduction is not consistent in space or time. This implies that a substantial part of the inter-product differences is instrument and/or retrieval-specific and the harmonization methods have limited application to TOAR II. An alternate method of combining the residual and profile products with a column fill-in method is expected to be published as the TOAR II "satellite assessment."

**1.2 TOAR II Studies with Ground-based Measurements. Statistical Issues.**

TOAR II has engaged a more globally representative set of researchers than TOAR I and reports data and analyses from a larger set of observations. Dozens of TOAR II-related publications can be reviewed at https://copernicus.org/articles/special_issue10_1256.html. Given the persistent uncertainty of the satellite records, a number of TOAR II contributors formed a community project, the Harmonization and Evaluation of Ground-based Instruments for Free-Tropospheric Ozone Measurements (HEGIFTOM), to apply newly standardized ozone measurement and processing protocols for data from sondes, aircraft and other ground-based (GB) instruments: FTIR, tropospheric ozone lidar and Umkehr retrievals from Dobson spectrometers. The rationale is that GB networks, with stable operations at fixed sites and well-calibrated instruments, e.g., as in the Network for Detection of Atmospheric Composition Change (NDACC; De Mazière et al., 2018), provide suitable time-series at dozens of sites over 7 continents and pole to pole. HEGIFTOM has two objectives: (1) harmonize data from ~80 long-term stations (1990s to 2023) in four GB networks using the most up-to-date reprocessing techniques with each record referenced to absolute standards; (2) calculate trends for the 2000 to 2022 period with harmonized data, reporting station trends with uncertainty. The trends for 55 individual stations are tabulated and illustrated in Van Malderen et al. (2025a; referred hereafter to as HEGIFTOM-1). Regional trends based on merging selected stations in densely sampled areas appear in Van Malderen et al. (2025b; referred hereafter to as HEGIFTOM-2).

Early in the TOAR II study period, in T21, we analyzed ozone profiles in the tropics collected in the Southern Hemisphere Additional Ozonesondes (SHADOZ) network (Thompson et al., 2003; Thompson et al., 2017) to compute FT and LMS ozone trends. The results in T21 are based on data from 8 combined SHADOZ stations within ±15 degrees latitude; the Goddard Multiple-Linear Regression (MLR)

198 model calculated trends from 1998 through 2019 from the surface to 20 km. Changes in individual

199 layers between 5 and 15 km were typically (5-10)%/decade, but only seasonally; over the equatorial SE

200 Asian stations at Kuala Lumpur and Watukosek, Indonesia, some layers displayed increases up to 20%/

201 decade (Fig. 6 in T21). However, in general, annually averaged changes in equatorial regions ranged

202 from ~0 to +(1-2)%/decade or –(1-2)%/decade. In T21 LMS ozone (LMS defined as within 15-20 km)

203 computed with the MLR model displayed a seasonal loss up to 10%/decade (July through September)

204 or to 3%/decade, annually averaged. The loss maximized at ~18 km. At the same time of year, a positive

205 trend in tropopause height (TH), derived from the SHADOZ radiosondes, was detected. Redetermining

206 LMS ozone changes in the 5 km column above the tropopause zeroed out the apparent trend.

207 More recently, the Stauffer et al. (2024, referred to as S24) paper demonstrated that over the 25-

208 yr period 1998-2022, early year (February through April/May) FT ozone increases in SHADOZ data

209 are associated with declining convection, most pronounced over SE Asia but observed to a lesser

210 degree at the other stations. With the newest OMI/MLS-based satellite estimates of total TrCO,

211 Gaudel et al. (2024) showed that over the Aura era (2005-2019) trends from satellite, SHADOZ and

212 IAGOS aircraft profiles were in good agreement with one another over southeast (SE) Asia, similar to

213 S24. SHADOZ only (T21) and IAGOS trends (Gaudel et al., 2024) diverge somewhat over the

214 equatorial Americas and Africa, partly due to a difference in sampling sites, e.g., west African IAGOS

215 profiles in Gaudel et al. (2024) versus the SHADOZ Nairobi station.

216 **1.3  This study**

217 We use the Goddard MLR model to calculate trends in monthly mean SHADOZ data for the

218 extended period 1998 through 2023, addressing the following questions:

219 - Compared to T21, that reported on the 1998-2019 period, what do FT and LMS ozone

220 trends look like in the equatorial zone (-15$^\circ$ to +15$^\circ$) with four additional years of SHADOZ

221 profiles? In other words, because the extension covers 2020 to 2023, the comparisons of 26-yr

222 trends with the 22-yr T21 record are looking for impacts of COVID-19 (Steinbrecht et al.,

223 2021; Ziemke et al., 2022).

224 - How do trends in tropospheric ozone for 1998-2023 compare to trends for 2000 to 2023?

225 In other words, is the 26-year trend biased by SHADOZ starting at the end of the 1997-1998 ENSO

226 that produced strong perturbations to tropical ozone (Thompson et al., 2001)?

227 - How do SHADOZ total tropospheric column (TrCO$_{sonde}$) changes compare to OMI/MLS

228 column ozone (Tr CO$_{satellite}$ ) trends over the 2005-2023 period? Do the satellite data capture the

229 seasonality of sonde-derived trends as noted in T21 and S24?

230 In addition to updated trends for equatorial SHADOZ sites, we have used SHADOZ profiles to

231 investigate three statistical issues raised in HEGIFTOM-1 and other TOAR II studies.

232    -    HEGIFTOM-1 calculated median trends for sondes and all other GB data using both Quantile
233        Regression (QR) and MLR models. Within the associated uncertainties of each, the two methods
234        gave identical results for annually averaged trends. Here we explore special features of QR and
235        MLR to learn more about the nature of the trends, e.g., seasonality (MLR), changes in the highest
236        and lowest quantile (QR).

237    -    Second, we use MLR to evaluate the sensitivity of trends on sample size as raised in TOAR II
238        papers (Chang et al., 2020; Chang et al., 2021; Gaudel et al. 2024) and HEGIFTOM-1 by
239        augmenting equatorial SHADOZ data with tropical IAGOS profiles for the appropriate region.
240        These calculations are carried out for FT ozone, i.e., in the region where radiative forcing is most
241        effective and both sondes and aircraft sample (700-300 hPa, roughly 5-10 km).

242    -    Satellite records are variable in length, with the most frequently used tropospheric estimates
243        starting after 2004 and a number of products merging measurements from multiple instruments.
244        We examine the sensitivity of trends to length of the observation period using QR by comparing
245        the 26-yr SHADOZ ozone trend to a recalculation that coincides with the IASI period 2008-2019
246        for which trends are reported in Boynard et al. (2025).

247     Data and analysis methods appear in **Section 2** with Results and Discussion in **Section 3. Section 4**
248    presents Summary and Conclusions.

249
250    **2.  Data and Methods of Analysis**

251    **2.1  Ozone datasets**

252     Three datasets are used in our study: ozonesonde profiles from the SHADOZ network; partial ozone
253    profiles from the IAGOS commercial aircraft network; monthly-averaged OMI/MLS tropospheric ozone
254    column estimates from 2005 through 2023.

255        **2.1.1  SHADOZ ozonesonde observations**

256    **Fig. 1a** displays the SHADOZ network stations, italicized with coordinates in **Table 1.** Quito (Cazorla,
257    2016; Cazorla et al., 2021; Cazorla and Herrera, 2022) and Palau (Müller et al., 2024) soundings, taken
258    since 2014 and 2016 respectively, have recently been added to the archive at
259    https://tropo.gsfc.nasa.gov/shadoz. The ozone profiles are obtained from ECC ozonesondes coupled to
260    standard radiosondes as described in earlier publications, e.g., Thompson et al., 2003; Thompson et al.
261    2007; Thompson et al., 2019. The profiles are archived with ozone uncertainties calculated with each
262    individual ozone partial pressure available as separate files at the SHADOZ archive (Witte et al., 2018;
263    WMO/GAW Rep. 268, 2021). Recent evaluations of ozonesonde data have established the quality of the
264    global ECC network. Measurements of TCO from 60 global ozonesonde stations average within ±2%
265    agreement with total ozone from 4 UV-type satellites since 2005 (Stauffer et al., 2022). About half of
266    SHADOZ stations exhibit a ~3-5% dropoff in stratospheric ozone (Stauffer et al., 2020) that is not

267  completely understood (Nakano and Morofuji, 2023; Smit et al., 2024). Accordingly, our study only uses

268  ozone data below ∼50 hPa, defining the lowermost stratospheric (LMS) ozone in 15-20 km.

269      For the update to T21, that was based on 1998-2019 SHADOZ V06 ozonesonde data

270  (https://doi.org/10.57721/SHADOZ-V06), the same records for 8 equatorial sites, located between 5.8N

271  and 14S (color-coded in **Fig. 1b;** italicized in **Table 1**) are used with four additional years (2020-2023)

272  of ozone and P-T-U (pressure-temperature-humidity) profiles. These 8 stations have at least 14 years of

273  data between 1998 and 2023, although several have multi-year gaps (**Figs. 2, 3 Fig. S1**). For more

274  reliable statistics three of the "stations" or "sites" as they are referred to (**Fig. 1b**), are defined by

275  combining profiles from pairs of launch locations abbreviated as follows: SC-Para for San Cristóbal-

276  Paramaribo (dark blue dots in **Fig. 1b**); Nat-Asc for Natal-Ascension (red dots in **Fig. 1b**); KL-Java (cyan

277  dots in **Fig. 1b**) for Kuala Lumpur-Watukosek (**Table 2**). T21 (see Supplementary Material) describes

278  multiple tests that were conducted to verify that these combinations are statistically justified. Annual

279  cycles in absolute column amounts (**Fig. 2**) and anomalies for the pairs were well-correlated. In T21

280  (Supplementary Material) total tropospheric columns integrated from sondes (TrCO$_{sonde}$) at the 8

281  individual stations were also well-correlated ($r^2$=0.72) with colocated TrCO$_{satellite}$ from OMI/MLS data

282  over the period 2005-2019. It is important to note that the 8 well-correlated sites are within 15 degrees

283  latitude of the equator. The correlation falls to $r^2$=0.50 when comparisons are made between sondes and

284  satellite columns for the 4 subtropical SHADOZ stations. FT ozone at those locations are seasonally-

285  dependent mixtures of tropical and extra-tropical air masses, with latitudes (**Table 4)** spanning Hanoi

286  (+21.0) to Irene (-25.9).

287      We have also analyzed trends of tropospheric ozone column and free tropospheric ozone at

288  individual SHADOZ stations using a QR model, following column definitions and guidelines for the TOAR

289  II/HEGIFTOM project analysis (Chang et al., 2023). The tropospheric ozone column in HEGIFTOM trends

290  analysis is defined as surface to 300 hPa; the FT is defined as a layer between 300 and 700 hPa and the

291  results are given as ppbv O$_3$/decade change and %/decade. The QR trends for 13 SHADOZ sites from

292  2000 to 2022 are summarized in **Table 4;** a subset of them appear in an evaluation of ground-based

293  global ozone trends in HEGIFTOM-1.

294      **2.1.2  SHADOZ and IAGOS-SHADOZ blended profiles. LMS and FT ozone**

295      The MLR trend analyses (results in **Table 2 and 3**) use SHADOZ profile measurements in several

296  ways.  First, the trends are computed using monthly-averaged ozone mixing ratios at 100-m intervals

297  from the surface to 20 km, as described in T21. Second, most results are illustrated as ozone column

298  amounts (in DU) for two FT segments, 5-10 km and 10-15 km, and for the LMS. Trends for ozone and P-

299  T-U data below 5 km are determined for completeness but are not tabulated because station sampling

300  times and local pollution can vary, giving artifact biases among the individual sites (Thompson et al.,

301  2014). We use 15-20 km for the LMS for two reasons. This is where several studies identified wave

302  activity associated with convection and ENSO-La Niña oscillations (Lee at al., 2010; Thompson et al.,

303  2011; Randel and Thompson, 2011; T21). Second, Randel et al. (2007) identified a distinct ozone annual

304  cycle in the 15-20 km range driven by the Brewer-Dobson circulation.

305      A third way of using SHADOZ profiles in the MLR analysis is in a blend with IAGOS aircraft profile

306  measurements within a lower FT pressure-defined region ("FTp" = 300-700 hPa, HEGIFTOM-1).

307  Calculations in the FTp segment are designed to add more samples within the SHADOZ-labeled

308  combination sites (compare profile numbers in **Tables 2 and 3**) and to augment regional trends in

309  HEGIFTOM-2 where no results are reported for the equatorial Americas, Atlantic Ocean or African

310  continent. In defining regions for merging SHADOZ and IAGOS observations, we follow locations

311  presented by Tsivlidou et al. (2023). Profiles from the SHADOZ Quito station (2014-2023) and two

312  IAGOS airports (Bogotá and Caracas) are added to the SHADOZ SC-Para profiles to define the equatorial

313  Americas for determining trends within the FTp (**Table 3**). Also, for the SHADOZ-IAGOS calculations,

314  sonde profiles from the Natal-Ascension pair are combined with 13 airports in west Africa (**Table 3**) to

315  determine trends for a region designated "Atlantic+West Africa," as shown in **Fig. 1b** (color-coded

316  circles) and the second column of **Table 3.** In "East Africa" Nairobi sonde data are combined with IAGOS

317  Nairobi and Addis Ababa ozone profiles. The FTp-designated Equatorial SE Asia consists of KL-Java

318  profiles from SHADOZ combined with IAGOS landing and takeoff data from Kuala Lumpur and

319  Singapore. Time-series of ozone column amounts (in DU and as anomalies) for SHADOZ stations and

320  airports for these 4 "regional" sites appear in **Fig. 3**. The coordinates of individual SHADOZ stations used

321  in the blended dataset (italicized) with IAGOS airports appear in **Table 1**. Calculations with FTp retain

322  Samoa as a single station.

323      **2.1.3  OMI/MLS satellite and sonde total ozone columns**

324      Trends computed with MLR for sonde-derived total tropospheric ozone columns (TrCO) are based on

325  integrating ozone mixing ratios from the surface to the thermal lapse-rate tropopause derived from the

326  radiosondes that accompany each ozonesonde launch. The standard WMO definition of tropopause is

327  used. For the 5 equatorial sites in our analyses, the tropopause is typically between 16 and 17 km. Our

328  $TrCO_{sonde}$ columns and trends are compared to $TrCO_{satellite}$, the tropospheric ozone columns estimated

329  from the OMI/MLS residual as described by Ziemke et al. (2019; updated in the TOAR II paper by Gaudel

330  et al., 2024). These newest OMI/MLR TrCO estimates have been corrected for a ~1%/decade upward

331  drift in OMI over the past two decades (Gaudel et al., 2024; SI material). The OMI/MLS column ozone

332  product is available starting in October 2004. We use monthly average TrCO for both sondes and

333  OMI/MLS between January 2005 and December 2023 **Fig. S1** in Supplemental Material. These are

334  identical to the data used in the Gaudel et al. (2024) TOAR II analyses of tropical ozone.

335      **2.2  Trend analyses**

336      **2.2.1 Multiple Linear Regression (MLR) model**

337    As in T21 and S24, the Goddard MLR model (original version Stolarski et al., 1991, updated in Ziemke

338    et al., 2019) is used for analysis of monthly mean ozone amounts. The MLR model includes terms for

339    annual and semi-annual cycles and oscillations prevalent in the tropics: QBO, MEI (Multivariate ENSO

340    Index, v2) and IOD DMI (Indian Ocean Dipole Moment Index; only for KL-Java):

341    $$O_3(t) = A(t) + B(t) + C(t)MEI(t) + D(t)QBO1(t) + E(t)QBO2(t) + F(t)IOD(t) + \varepsilon(t)$$

342    where t is month.  The coefficients are as follows: A through F include a constant and periodic

343    components with 12, 6, 4, and 3 month cycles, where A represents the mean monthly seasonal cycle and

344    B represents the month-dependent linear trend. When annual trends are reported, the B term includes

345    only the 12-month component to generate a single trend value over the period of computation. The

346    model includes data from the MEIv2 (https://www.esrl.noaa.gov/psd/enso/mei/), the two leading QBO

347    EOFs from Singapore monthly mean zonal radiosonde winds at 10, 15, 20, 30, 40, 50, and 70 hPa levels,

348    and IOD DMI (https://psl.noaa.gov/gcos_wgsp/Timeseries/Data/dmi.had.long.data).  The $\varepsilon(t)$ is the

349    residual, i.e., the difference between the best-fit model and the raw data. T21 noted that the monthly

350    ozone data and MLR model fits for the mid FT (5-10 km) and LMS layers are well-correlated. For the

351    LMS, for example, the correlation coefficients are r = 0.83-0.90 (**Fig. S7** in T21). The IOD DMI term is

352    included for KL-Java, the only station where the IOD impact on the ozone trend is reliably detected.

353    The 95% confidence intervals and p-values for each term in the MLR model as presented here are

354    determined using a moving-block bootstrap technique (10,000 resamples) in order to account for auto-

355    correlation in the ozone time series (Wilks, 1997). The model is applied to ozone anomalies in all cases

356    in order to minimize biases that might arise from intersite ozone differences between pairs for the

357    combined stations: SC-Para, Nat-Asc, KL-Java (**Table 2**). In other words, we calculate ozone anomalies

358    from the individual station's monthly climatology for all profiles before combining the pairs into

359    monthly means and computing the MLR ozone trends. Anomalies are also analyzed for the Nairobi and

360    Samoa station data, although this would be no different than computing MLR trends on the actual ozone

361    timeseries themselves. The MLR model was separately applied to the monthly mean ozone profile

362    anomalies at 100 m resolution, and the monthly mean partial column ozone anomaly amounts from 5-

363    10 km, 10-15 km, and 15-20 km. The MLR model was also applied to the monthly mean tropopause

364    height (TH) anomaly at each station, defined as the 380 K potential temperature surface (e.g., Wargan et

365    al., 2018).  Because TH and LMS ozone trends turn out to be strongly correlated (T21), the MLR analysis

366    was also performed for the ozone column amount anomalies referenced to the tropopause.  In that case

367    LMS ozone trends refer to changes in the 5 km above the tropopause with the FT extending from the

368    tropopause to 5 km below the tropopause (**Section 3, Table 2)**. Finally, the MLR model was applied to

369    total tropospheric column amounts from the sondes (TrCO$_{sonde}$) and corresponding TrCO$_{satellite}$ from

370    OMI/MLS (surface to Tp in **Table 2)**.

371     Note that recent ozone trend studies and the TOAR II guidelines (Chang et al., 2020; Cooper et al.,

372     2020; Chang et al., 2023) have discouraged the use of nomenclature associated with statistical

373     significance whereas the Figures and Tables presented here refer to trends using terminology of 95%

374     confidence intervals (equivalent to p-value < 0.05), the most reliable results in **Section 3** (bold in

375     **Tables 2, 3** and **4)** are explicitly stated as based on p-values < 0.05.

376     Several studies of tropospheric ozone observations have noted a persistence of COVID-19

377     perturbations on ozone trends after 2019 (Ziemke et al., 2022; HEGIFTOM-1; HEGIFTOM-2). A

378     comparison of the extended SHADOZ mean ozone trends (1998-2023) relative to those from T21

379     (covering 1998 to 2019), both summarized in **Table 2,** represents the impact of COVID-19 in the deep

380     tropics. Likewise, SHADOZ was initiated at the end of the powerful 1997-1998 ENSO. Accordingly, we

381     applied MLR to the same 5 sites for 2000-2023 to evaluate any artifacts relative to the 1998 to 2023

382     trends. Those results also appear in **Table 2.**

383     **2.2  Quantile Regression (QR) model**

384     Whereas MLR has been the standard tool for analyzing global total and stratospheric ozone trends, the

385     latter often with satellite data where zonal means can be used, the TOAR II project has recommended

386     using QR as better suited for ozone trends in the troposphere where, for example, urban concentrations

387     can vary by factors of 3-4. Because it is a percentile-based method (Koenker, 2005), the heterogeneously

388     distributed changes of trends can be estimated, as shown, for example, in Gaudel et al. (2020).  To date

389     the TOAR II HEGIFTOM trends studies for observations at individual sites (HEGIFTOM-1) and regionally

390     organized data (HEGIFTOM-2) have been studied with the QR approach. In those studies and for the 13

391     individual SHADOZ time-series (**Table 4**) QR has been applied to the median change of the trends,

392     which is equivalent to the least absolute deviation estimator (i.e. aiming to minimize mean absolute

393     deviation for residuals; Chang et al., 2021). The rationale is that compared to least-squares criterion, a

394     median-based approach is more robust when extreme values or outliers are present. Median trends are

395     estimated based on the following multivariate linear model:

396     Observations[t] = a0 + a1*sin(Month*2$\pi$/12) + a2*cos(Month*2$\pi$/12)

397     + a3*sin(Month*2$\pi$/6) + a4*cos(Month*2$\pi$/6) + b*t + c*ENSO[t] + N[t],          Eq. 1

398     where harmonic functions are used to represent the seasonality, a0 is the intercept, b is the trend value,

399     c is the regression coefficient for ENSO, and N[t] represents the residuals. Autocorrelation is accounted

400     for by using the moving block bootstrap algorithm, and the implementation details are provided in the

401     TOAR statistical guidelines (Chang et al., 2023).  In the individual site analyses of HEGIFTOM

402     observations (HEGIFTOM-1), where all individual ozone records (designated as L1) and monthly means

403     (denoted as L3) were analyzed, annually averaged trends turned out to be the same within

404     uncertainties. Where QR is applied in the present study, L1 ozone data are used.

405     **2.2.3  Trend Sensitivity Studies**

406    Three sensitivity studies were conducted, related to (1) sampling frequency; (2) the complementarity

407    of MLR and QR methods; (3) duration of time-series.

408    A number of TOAR-related studies (Chang et al., 2020; Chang et al., 2021; Chang et al., 2023) have

409    emphasized links between ozone time-series sampling characteristics, i.e., frequency of profile

410    measurements and/or temporal gaps, and trend uncertainty. Gaudel et al. (2024), for example, show

411    uncertainty (as 2-sigma) in median tropospheric ozone profiles; the inference is that 6-15 monthly

412    samples are required for meaningful FT trends (Fig. 1-2 in Supplemental Material, Gaudel et al., 2024).

413    For the first sensitivity test we examined trends dependence on sample size by comparing the annual

414    trends computed with MLR for the lower-mid-FT ozone segment (5-10 km) to the trends from the

415    combined SHADOZ-IAGOS merged monthly mean SHADOZ profiles (L3, 700-300 hPa) for 1998-2023. A

416    comparison of **Tables 2** and **3** indicate that for the equatorial Americas and Atlantic regions, the sample

417    numbers are increased more than a factor of 2; the other two sites have enhancements of 1.3 and 1.5.

418    The results in DU/decade and %/decade, appear in **Table 3.**

419    In the second sensitivity study three calculations were made using the data from all individual

420    SHADOZ stations as in HEGIFTOM-1, not only the 5-site equatorial profiles (**Table 2)**. The individual

421    station results appear in **Table 4.** The trend (1998-2023) in mean tropospheric column, TrCO (in

422    DU/decade), was computed using the QR method applied to all profiles at each station (L1, level 1 data)

423    with median (50%-ile) trends shown. The L1 sample numbers ranged from 326 (Watukosek) to 1142

424    (Hilo); the L1/L3 sample size ratios ranged from 2.2 to 4.3 with only 3 of 13 stations having a ratio

425    below 3.2 (i.e., fewer than 3 profiles per month). These trends can be compared to the MLR trends in

426    **Table 2.**  The second calculation was a computation of trends at each station for the FTp column amount

427    used in HEGIFTOM-1(700-300 hPa, comparable to our 5-10 km segment in **Table 2** and the combined

428    IAGOS+SHADOZ FTp columns in **Table 3**). HEGIFTOM-1 pointed out the complementarity of applying

429    both MLR and QR to the 23-yr time-series of mean ozone column amounts. The advantage of MLR is a

430    graphical display of monthly trends that indicate important ways ozone interacts with seasonally

431    varying dynamics, as in S24 or Millet et al. (2025). QR distinguishes trends among different segments of

432    the distribution, an advantage for stations where tropospheric ozone segments are highly variable. To

433    demonstrate this, the QR method (including trends for the 5%-ile, 25%-ile, 75%-ile, 95%-iles) was

434    applied to IAGOS+SHADOZ combined FT dataset for the four regions: equatorial Americas;

435    Atlantic+West Africa; East Africa; equatorial southeast Asia.

436    The third sensitivity test investigates the degree to which trends and uncertainties depend on the

437    length of sampling. This issue arises because the most frequently used satellite estimates of

438    tropospheric ozone begin after 2003 compared to SHADOZ (1998-) and IAGOS (1994-). The Boynard et

439    al. (2025) study uses IASI products for 2008-2019 (and 2008-2023), comparing only 7 of ~40 potential

440    ozonesonde stations for evaluation. Using L1 mean TrCO tropospheric columns, the QR method was

441    applied to the 13 SHADOZ stations for a 12-year period (2008-2019) for comparison. The results in

442    **Table 5** demonstrate the impact of sampling in a shortened time series.

443

## 3  Results and Discussion

### 3.1  Monthly and seasonal ozone climatology at 5 SHADOZ sites

446    **Figure 4** displays the 5-site monthly ozone climatology based on SHADOZ monthly averaged data

447    from the surface to 20 km. Regional differences in vertical structure within the FT are pronounced. For

448    example, the contours representing the 60-90 ppbv range (yellow to red colors) are absent in mid-FT

449    ozone over KL-Java or Samoa (**Figs. 4d,e**). Conversely, FT ozone values ≤ 30 ppbv (darkest blue shades)

450    observed over KL-Java and Samoa in the middle FT never appear over the other 3 stations: equatorial

451    Americas (SC-Para, **Fig. 4a**), Nat-Asc or Nairobi (**Figs. 4b,c**). These contrasts may reflect regional

452    differences in ascending vs. descending nodes of the Walker circulation. The latter feature is partly

453    responsible for the tropospheric zonal wave-one (Thompson et al., 2003) that refers to a mean TrCO

454    over the south tropical Atlantic Ocean that is sometimes twice as large as over the western Pacific. There

455    is less regional variability in LMS ozone. At all stations (**Fig. 4**) above ~16 km the colors and contours

456    are nearly uniform over the year. Mixing ratio contours of 100 ppbv and 200 ppbv may appear as a thick

457    white line. The 100 ppbv level is sometimes referred to an ozonopause; typically it is within 1-2 km of

458    the thermal lapse-rate tropopause.

### 3.2   FT and LMS ozone annual cycle (1998-2023)

460    The annual cycle of ozone at the two FT layers and for LMS ozone appear as anomalies in **Fig. 5.** FT

461    ozone seasonality (**Figs. 5a,b**) is less uniform than for LMS ozone (**Fig. 5c**) and tropopause height (TH,

462    **Fig. 5d**). Randel et al. (2007) showed that the near-uniform LMS ozone seasonality in the equatorial

463    zone is due to the Brewer-Dobson circulation. The more varied FT ozone cycles in **Figs. 5a,b** are due to a

464    range of different dynamical and chemical influences across the stations. As expected, the annual cycles

465    for the pressure- and regionally defined FTp ozone (**Fig. 6** in %**)** resemble those for the corresponding

466    SHADOZ sites in the lower (5-10 km) FT layer in **Fig. 5a**; the magnitudes are similar as well although

467    **Figs. 5** and **6** are illustrated with different scales. In both cases it is seen that there are two seasonal

468    maxima and minima for KL-Java (**Fig. 5a)** and equatorial SE Asia (**Fig. 6a**). The early year minima are

469    associated with intense convective activity (T21, S24) that repeats in August at the onset of the Asian

470    monsoon. KL and Watukosek are also affected by seasonal fire activity at the latter end of the rainy

471    seasons. These features were described in detail in Stauffer et al. (2018) using Self-Organizing Map

472    clusters and proxies for convection and fires.

473

### 3.3  FT ozone trends: regional and seasonal variability

475    #### 3.3.1  Trends for 1998-2023

13

In **Fig. 7** the trends in %/decade computed with MLR at 100-m intervals, for 1998 to 2023, are displayed (update of Fig. 6 in T21 for the 1998-2019 trends). Changes in the ozone column amounts for 1998-2023 computed from the model (DU/decade and %/decade) for the two FT layers (5-10 km, 10-15 km) appear in **Fig. 8**. A summary of values for the two layers (and for LMS ozone) appears in **Table 2.** The percentage values in **Fig. 7** and **Table 2** are the result of dividing the MLR B(t) term by the A(t) annual cycle of ozone term (Section 2.2.1). The MLR-calculated A(t) annual cycle derived from monthly mean ozone profiles (i.e., no anomaly calculation) is used to convert the B(t) trend in ppmv/decade (profiles) or DU/decade (partial columns) to %/decade. Ozone trends for both percent/decade and DU/decade are given in **Table 2.** Shades of red (blue) in **Fig. 7** represent ozone increases (decreases); cyan hatching denotes trends with p-values < 0.05. The annual mean trends in **Table 2** are computed by taking the average of the 12 monthly trends in DU and dividing by the mean seasonal ozone in DU to yield the annual percentage trend.

For 3 of 5 stations in **Figs. 8a** and **c**, there is a pattern of ozone increase at both FT layers in January to April. Percentage-wise the greatest increases are at KL-Java and Nairobi, ~(10-15)%/decade in March and April. However, SC-Para and Samoa at 5-10 km (**Fig. 8a)** exhibit almost no trend at any time of year; at 10-15 km SC-Para and Nairobi show losses up to 10%/decade in February and (5-10)%/decade losses in August and September. However, **Table 2** displays no trend on an annual basis for SC-Para and Nairobi. Inspection of **Fig. 7** suggests small FT trends at Nat-Asc; **Table 2** displays a +3.4%/decade increase in the 10-15 km layer from 1998-2023. The total column, integrated to the tropopause, TrCO (**Fig. 9**) over Nat-Asc, has increased (1.9± 1.8)%/decade, p<0.05. There are no other annually averaged trends in the FT layers but TrCO for KL-Java (KL-Watukosek in **Table 2**) also increased, (2.6± 2.3)%/decade.

### 3.3.2 FT ozone trends sensitivity to COVID-19 and 1997-1998 ENSO

A comparison of the **Table 2** columns for 1998-2023 relative to those for 1998-2019 (the latter is from T21) reveals little. Only the 10-15 km layer at Nat-Asc has entries with p<0.05 for both periods. The extra 4 years reduced the positive trend slightly. This is consistent with studies that found lingering COVID-related declines in sondes and satellites (Ziemke et al., 2022; HEGIFTOM-1). In **Table 2** columns for trends for 2000-2023 can be compared to those for 1998-2023. There is little information in the 2000-2023 column, i.e., no trends anywhere except for the TrCO for KL-Java, an area that was well-studied with satellite and some sonde measurements for the period affected by the large ENSO, amplified by the Indian Ocean Dipole pattern (Thompson et al., 2001). After August 1997, as a result of exceptionally high fire activity, ozone increased greatly. That could have meant a smaller change between ozone levels from 1998 through 2023 which would be consistent with a larger, more robust trend for 2000-2023 (4.6%/decade for KL-Java) compared to T21, 2.6%/decade (both p<0.05). Similar

510  trend differences for Kuala Lumpur are also observed with the QR trends in HEGIFTOM-1 (~4-

511  5%/decade for 2000-2022) versus 2.7%/decade in **Table 4**.

512

513  **3.4  LMS ozone trends and mean vertical trend over 5 SHADOZ sites**

514  In T21 (Figs. 10 and 11) trends in the LMS (nominally 15-20 km) showed 5-10%/decade decreases for

515  Nat-Asc, KL-Java and SC-Para between July and October. For the same months those locations exhibited

516  a tropopause increase ~100 m/decade, suggesting that the seasonal ozone increase is an artifact of a

517  changing tropopause. In other words, if the TH increased more air with relatively lower ozone would be

518  located in the 15-20 km layer. We tested this hypothesis by recomputing ozone column changes

519  referenced to the TH for 1998-2019, i.e., evaluating trends in a 5-km thick layer above the TH. The result

520  was that the apparent loss of LMS ozone from July to September or October disappeared. The same

521  analyses performed with LMS ozone and TH for the 1998-2023 period (**Fig. 10)** are the same as for

522  1998-2019 (T21).

523  Whatever the cause(s) of ozone loss in the LMS, it is a feature clearly captured by SHADOZ data as seen

524  in annually averaged ozone trends derived from the analyses displayed in **Fig. 11.** At 18 km the

525  composite trend from the 8 SHADOZ stations analyzed with MLR is (-4±3)%/decade. The mean trend

526  from ~13 to 3 km is zero, albeit with a ±2σ (95%) ±%/decade. Only below ~2km is the mean ozone

527  trend clearly positive. Most of that increase originates from near-surface pollution over equatorial SE

528  Asia (Fig. 6 in S24).

529  **3.5  Sensitivity tests.  Trends method.  FT sample numbers.  Length of time-series**

530  **3.5.1  Complementarity of Trends Methods**

531  In **Table 4** the median (50%-ile) QR trends from 1998-2023 for the TrCO and FTp ozone segments

532  for the 13 individual SHADOZ stations are presented.  The trends for the tropical stations are

533  comparable to the MLR trends in **Table 2 and 3**, respectively, within their uncertainties, reaffirming the

534  important HEGIFTOM-1 conclusion, i.e., MLR and QR trends from ground-based data (FTIR and Umkehr,

535  as well as sondes) are essentially the same. In **Fig. 12** the timeseries and histograms show the

536  distribution of IAGOS+SHADOZ ozone anomalies (in DU) for the four regions. The median trends from

537  1998 to 2023 (50%-ile) for the FTp ozone segments are also displayed with the lowest and highest (5%,

538  95%, respectively), 25%-ile and 75%-ile quantiles with red circles denoting p< 0.10. The medians are

539  statistically nearly the same, although as expected, the 2-σ uncertainty bars are smaller with the QR

540  method than with MLR. The MLR trends are higher in all cases except the equatorial Americas (**Fig.**

541  **12a**). In the latter case, the positive anomalies have increased significantly for the 5% and 25%

542  quantiles over the 26-yr period with no change for the 50%, 75% or 95% quantiles. This signifies that

543  the background (lowest-ozone) air has increasing ozone but the highest-ozone distribution has not

544  changed. Over the Atlantic+West Africa (**Fig. 12b)** there are also small increases in the lowest part of the

distribution but the median and higher %iles show no change. Note Natal alone (when not combined with other stations) shows high confidence increases in FTp (and TrCO) ozone (**Table 4**). East Africa (**Fig. 12c**) shows marked increases in the lowest-ozone quantiles and the median but a significant decrease in the highest-ozone (more polluted) air. The opposite is true over equatorial southeast Asia (**Fig. 12d**). The most polluted air corresponds to ozone increasing but the background (lowest ozone) FT segment shows an ozone decrease.

### 3.5.2  FT sample numbers

**Figure 13** monthly ozone trends are based on a total of 1.8 times the number of profiles as those in the other lower FT layer, **Fig. 8a** and **8b.** For the equatorial Americas (blue) twice as many profiles contribute to the trends in **Fig. 13** than in **Figs. 8a** and **8b;** for the Atlantic+West Africa includes 2.5 times more profiles than in **Figs. 8a** and **8b.** In all four regions, the seasonality of the trends is nearly the same between the 5-10 km FT segment (**Figs. 8a** and **8b)** and the corresponding SHADOZ+ IAGOS trend **(Fig. 13).** Furthermore, month by month, the trends are similar to those in the 5-10 km layer in both magnitude and confidence level (uncertainty). **Table 3** shows no trends ($p < 0.05$) at any location. The null trends are illustrated in the annual means at the right of each image in **Figs. 8** and **13**. This was unexpected given the Chang et al. (2023) and Gaudel et al. (2024) suggestions that the uncertainty should decline with more samples and positive trends might be amplified.

### 3.5.3  Length of time-series

**Table 5** displays a comparison of TrCO trends determined by QR for the SHADOZ 26-yr period, 1998-2023 for 13 individual SHADOZ stations, and for the same time-series only between 2008 and 2019. The uncertainties (expressed as $\pm 2\text{-}\sigma$) increased by factors of 2-3 or more for 10 of 13 stations. These results are based on a Comment on Boynard et al. (2025) that also compared the time-series changes for 17 mid-latitude ozonesonde stations. Similar uncertainty increases were noted for all 27 stations. Of that total, 9 stations exhibited ozone trend sign changes with the 12-year time-series although only 10 trends were statistically significant. In **Table 5** 2 stations change sign in their trends, 3 stations have a change in confidence level ($p < 0.05$); note that 8 of 13 stations exhibit a substantial change in their trend value, e.g., Samoa, Ascension Island. These results reinforce the need for multi-decade time-series.

### 3.6 Total tropospheric ozone trends, TrCO (1998-2023), from OMI/MLS and SHADOZ

Trends for the most recent version of OMI/MLS TrCO$_{satellite}$ are based on monthly mean satellite data and determined with MLR over the period 2005 through 2023. Trends for total tropospheric column ozone (TrCO$_{sonde}$) at the 5 SHADOZ sites for the same period appear in circles on the map in **Fig. 14** where the stippling indicates no trend can be determined. For both OMI/MLS and the sondes (**Fig. 7**) shades of red indicate total column ozone increases; blue represents declining ozone over the period of analysis. The mean annual TrCO$_{sonde}$ trends appear in the two rightmost columns in **Tables 2** and **6.** In

580 **Fig. 14** OMI/MLS shows trends > 1 DU/decade (typically 2-9%/decade) only appear over equatorial SE

581 Asia and parts of South America and the eastern Pacific at ~5N latitude. Circles indicate locations and

582 trends for the individual SHADOZ stations. The SHADOZ trends display lower trends than OMI/MLS. On

583 a month-by-month basis, the sonde and OMI/MLS trends are compared in **Fig. 15.** In 3 cases the

584 seasonality of TrCO trends from sonde and OMI/MLS are similar and the annually averaged OMI/MLS

585 TrCO$_{satellite}$ trends are not different from zero (symbols at right of each image). The seasonality of the KL-

586 Java monthly trends agrees well with OMI/MLS; the satellite mean is +5%/decade, gray in **Fig. 15d**. The

587 sonde SC-Para trend (**Fig. 15a; Table 6**) is quite a bit lower early in the year than the OMI/MLS trends

588 over San Cristóbal and Paramaribo that average +(2-3)%/decade. The Samoa sonde trend and OMI/MLS

589 TrCO trends diverge most of the year. The satellite annual trend is close to +10%/decade, an outlier

590 globally (HEGIFTOM-1) as well as over the tropics where no ground-based study results in a significant

591 trend for TrCO$_{sonde}$ over Samoa (**Section 4.2**).

592 **4  Summary and Conclusions**

593 We have presented a two-part evaluation of tropical ozone trends using a 26-yr record of

594 ozonesonde (SHADOZ, 1998-2023) profiles with selected FT aircraft (IAGOS) ozone data and the most

595 recent OMI/MLS estimates of tropospheric column ozone for 2005-2023. The next section summarizes

596 the findings. It is followed by **Section 4.2** which compares our trends to related TOAR II studies. **Section**

597 **4.3** concludes with a consensus view of FT ozone trends and perspectives relevant to the overall TOAR-

598 II climate and tropical assessments.

599 **4.1  Summary of findings**

600 The first part of the study updates trends in FT and LMS ozone for 5 stations, Nairobi, Samoa and

601 three combination sites (San Cristóbal-Paramaribo, Natal-Ascension, Kuala Lumpur-Watukosek)

602 extending the T21 trends, that covered 1998-2019, by 4 years. The new analysis added monthly

603 averaged data from 2000 to 2023 to the Goddard MLR model with standard proxies. Trends in FT (5-

604 10km, 10-15 km) and LMS (15-20 km) layers are illustrated with monthly means and annually averaged

605 changes in DU/decade and %/decade. Trends determined for the period 2000-2023 assessed impacts of

606 the 1997-1998 ENSO on a possible anomalous starting point. Comparisons of trends for the monthly

607 averaged Aura-derived OMI/MLS total tropospheric column ozone product (TrCO$_{satellite}$) were made to

608 those from monthly sonde-derived TrCO$_{sonde}$ for 8 equatorial SHADOZ stations. The principal results of

609 the SHADOZ trend updates and comparisons are as follows:

610 • The overall characteristics of T21 trends in the FT and LMS are confirmed with 4 additional years

611 of SHADOZ observations. From 1998 to 2023, regional and seasonal variability remains

612 pronounced with FT ozone increasing in thin layers at 4 of 5 SHADOZ stations ~(5-20)%/decade,

613 mostly between January and May. The exception is at SC-Para where there was a 5-10% ozone

614 decrease between 10-15 km during 1998 to 2023 compared 5-10%/decade increases in 1998-

17

615  2019 (T21). For 1998-2023, the greatest ozone increases occur in multiple layers below 10 km

616  over Nairobi and KL-Java and between 10-15 km over Samoa. However, these features do not

617  translate into annually averaged trends ($p<0.05$) in the 5-10 km or 10-15 km segments except

618  over Nat-Asc, i.e., adding 4 years of data to equatorial SHADOZ data does not modify the T21

619  picture of little or no FT ozone change. Only when the total tropospheric column ($TrCO_{sonde}$) trend

620  is evaluated do Nat-Asc (1.9±1.8)%/decade and KL-Java (2.6±2.3)%/decade) exhibit the slightest

621  trend ($p<0.05$). Examining the 5-station average in vertical form shows a null trend from ~3 to

622  17 km (0±2% within 2σ up to 7 km and ~0±3% from 7 to 17 km). The marginal overall mean

623  increase, +5%/decade below 3 km, is primarily driven by KL-Java changes.

624  • With the starting year delayed to 2000, the $TrCO_{sonde}$ KL-Java trend (2000-2023) is almost twice

625  as large as for 1998-2023, indicating an effect of the 1997-1998 ENSO on equatorial SE Asia. This

626  is not surprising. Watukosek soundings (1997-1998) show ENSO-induced anomalously high

627  ozone over Indonesia that was also captured by satellite tropospheric ozone estimates from

628  TOMS (Thompson et al., 2001).

629  • The T21 LMS ozone and TH trends are also confirmed with 4 more years of data. For the layer 15-

630  20 km, ozone losses ~5%/decade from June through October, on average, give an all-site average

631  of -3%/decade at 17.5 km, a value similar to satellite averages (Godin-Beekmann et al., 2022). As

632  in T21, re-determining the LMS trends for an ozone column 5 km above the tropopause from

633  1998 to 2023, causes the trend to disappear.

634  • Annually-averaged trends, 2005-2023, determined with MLR for OMI/MLS columns, $TrCO_{satellite}$,

635  over the 8 individual equatorial SHADOZ stations (members of the 5 combined sites) and

636  $TrCO_{sonde}$ overlap within the uncertainties of each. Trends are close to zero at Nat-Asc, Nairobi

637  and KL-Java. The OMI/MLS $TrCO_{satellite}$ trends are marginally positive at SC-Para, with monthly

638  cycles diverging in the early part of the year at SC-Para. OMI/MLS trends do not capture large

639  monthly seasonal variations seen in SHADOZ profiles, especially for negative trends. The large

640  positive trend from OMI/MLS over Samoa does not align with determinations of FT ozone from

641  this or other studies (see below).

642  The second part of the investigation was motivated by statistical issues raised in related TOAR II

643  trends analyses. The results of these analyses are summarized:

644  • Trends methods. The relative merits of trends computed with QR and MLR, previously

645  demonstrated in HEGIFTOM-1, were reinforced with analysis of combined FT SHADOZ-IAGOS

646  data. Although median trends are the same, QR uncertainties are smaller. MLR is superior for

647  capturing seasonal influences but QR provides vital information on whether the background, low-

648  ozone or high-ozone (polluted) populations are changing the most.

649      • <u>Sampling frequency.</u> The sensitivity of the 1998 to 2023 FT ozone trends to sample number was

650         explored by using IAGOS profiles to increase the SHADOZ sample size for the equatorial stations

651         by 80% overall, including a doubling over the equatorial Americas and Atlantic regions, then

652         applying MLR. Median trends were nearly unchanged. No FT trends over the 4 regions (plus

653         Samoa) are detected with $p < 0.05$ although uncertainties, expressed in ppbv/decade, improved

654         30% over the equatorial Americas and by ~15% over 3 of the 4 other sites. These results indicate

655         that current SHADOZ sampling is sufficient in this radiatively-important region.

656      • <u>Length of trends.</u> These were examined for the individual station $TrCO_{sonde}$ trends by comparing

657         trends for 1998 to 2023 with a 12-year trend (2008-2019), one of two scenarios investigated by

658         Boynard et al. (2025). The uncertainties (as 2-σ limits) increase by a factor of 2-3 for TrCO at 10

659         of 13 SHADOZ stations and some median trends change sign compared to the 26-year trends

660         (**Table 5**). The next section shows that even 16-year IASI/Metop trends have an unreasonably

661         low bias with respect to SHADOZ, IAGOS and OMI/MLS trends (**Table 6**), reinforcing a need for

662         multi-decade datasets given that FT ozone changes are relatively small.

663

664   **4.2 Comparison of this study to related TOAR-II investigations**

665   How do our tropical tropospheric ozone trends compare to those in other studies that use SHADOZ

666   and IAGOS profiles and/or satellite data?  **Table 6** summarizes our results for the FT, UT segments and

667   for TrCO. The FT ozone comparisons are made with Gaudel et al. (2024) and with results for two

668   HEGIFTOM studies (HEGIFTOM-1; HEGIFTOM-2). For UT ozone, SHADOZ trends are compared to those

669   derived from the lowest 3 layers of MLS (Froidevaux et al., 2025; see their Table 2). TrCO trends are

670   taken from the 5 SHADOZ stations, OMI/MLS (this study) and IASI/Metop (Boynard et al., 2025). Note

671   that the latter study only spans 2008-2023, much less than the SHADOZ data but close to the OMI/MLS

672   period, 2005-2023.

673   The tropical trends study of Gaudel et al. (2024) groups SHADOZ and IAGOS profiles somewhat

674   differently from this study and only extends through 2019 (period of trends are shown in the 4th column

675   of **Table 6**). Our trends and those of Gaudel et al. (2024) for $TrCO_{sonde}$ (**Table 6, Fig. 16a**) for the

676   equatorial Americas fall within range of one another. They fall within the wide range of the satellite

677   products: (3.1±2.5)%/decade for OMI/MLS (2005-2023) and (-4.0±1.1)%/decade for IASI/Metop

678   (2008-2023), an offset of 7.1%/decade for the median trends.  The equatorial Americas FT ozone trends

679   range from (-0.01%/decade to -3.3%)/decade (**Fig. 16b**).

680   For the Atlantic and western Africa regions, the profile-based comparisons differ in station-airport

681   combinations among our study and analyses in Gaudel et al. (2024), HEGIFTOM-1 and HEGIFTOM-2. The

682   TrCO and FT trends (**Table 6, Figs. 16a** and **16b**) among the 4 studies fall in a relatively small range: (-

683   1.3±2.8)%/decade (Gaudel et al, 2024) to (1.9±2.2)%/decade (this study) for FT and (-

684     1.1±0.9)%/decade (Gaudel et al, 2024) to (1.9±1.8)%/decade (this study) for TrCO. The larger TrCO

685     from the Natal-Ascension combination appears to result from a higher positive trend in the UT

686     (3.4±2.9)%/decade (**Fig. 16c**). Because the FT ozone trend of Gaudel et al. (2024) is negative and the

687     Nat-Asc FT ozone trend is positive (**Table 6**), combining western African IAGOS profiles with the Natal

688     and Ascension measurements, reduces the larger area trend compared to the sonde-only FT ozone

689     trend. **Table 6** shows that for all regions the MLS-derived UT ozone trend estimates fall between

690     +3%/decade and +4%/decade (Froidevaux et al. 2025). Only over the Atlantic region do any of the

691     SHADOZ UT ozone trends fall in this range (**Fig. 16c**). Overall, the Atlantic and western Africa FT ozone

692     and $TrCO_{sonde}$ trends are 0-2%/decade, in agreement with OMI/MLS (1.3±1.4)%/decade. As for the

693     equatorial Americas, the 2008-2023 trends from IASI/Metop over the Atlantic and western Africa is

694     much lower: (-4.9±2.0)%/decade. Compared to the OMI/MLS trend, the IASI/Metop median trend is

695     lower by 6.2%/decade. The picture for east Africa (both SHADOZ and IAGOS profiles over Nairobi) is

696     similar to the Atlantic and western Africa. FT ozone, $TrCO_{sonde}$ and OMI/MLS TrCO trends are essentially

697     null, similar to HEGIFTOM (**Table 6, Figs. 16a** and **16b**) but IASI/Metop displays a (-3.6±1.0)%/decade

698     trend.

699         There is more variability in trends among the ground-based studies for the equatorial SE Asia region

700     than the equatorial Americas, Atlantic and Africa, most likely because different combinations of IAGOS

701     profiles and SHADOZ data were used. Supplementing FT KL-Java SHADOZ profiles with IAGOS data

702     (**Tables 3** and **6**) in our study, a 50% increase in sample size, did not change the trend appreciably:

703     (1.0±2.5)%/decade vs (1.6±3.2)%/decade. The corresponding $TrCO_{sonde}$ over KL-Java increased

704     (2.6±2.3)%/decade. S24 computed trends with MLR for KL-Java for 1998-2022: the $TrCO_{sonde}$ was

705     (3.4±2.6)%/decade. Although the trend period only differs by one year, the smaller trend with the extra

706     year in this study (to 2023) might reflect some COVID impact (columns 5 and 7 in **Table 2**). For

707     OMI/MLS TrCO, determined from a mean of changes averaged over $5^{o}$x$5^{o}$ grid boxes for KL and

708     Watukosek (Java), there was a (5.6±6.0)%/decade, 2005-2023. The latter change is nearly the same as

709     Gaudel et al. (2024) for both FT ozone and OMI/MLS changes over the same interval. There are several

710     reasons for why Gaudel et al. (2024) FT ozone trends in **Table 6** and **Fig. 16b** are larger than our

711     SHADOZ-IAGOS FT ozone trends. First, the fusing of SHADOZ and IAGOS profiles in Gaudel et al. (2024)

712     may be more heavily weighted to polluted IAGOS segments than our merging. Second, reprocessed

713     IAGOS profiles have not been rigorously compared to SHADOZ data up to this point; a new evaluation of

714     IAGOS instrumentation in the World Calibration Center for Ozonesondes may facilitate consistent

715     referencing to an absolute ozone standard in the future (Smit et al., 2024; Smit et al., 2025). Third, with

716     the shorter trend period ending in 2019, the data of Gaudel et al. (2024) would not be affected by lower,

717     COVID-perturbed ozone concentrations in 2020-2023 as some SHADOZ records were (**Table 2**).

The HEGIFTOM-1 FT ozone trend (2000-2022) for Kuala Lumpur is nearly identical to the KL-Java trend, 1998-2023: (2.2±3.0)%/decade. In HEGIFTOM-2 (based on SHADOZ KL and IAGOS from several SE Asia airports) FT ozone increases over a longer period (1995-2022) are (6.2±2.2)%/decade. Thus, in general, over SE Asia, as for the equatorial Americas, Atlantic and Africa, the GB and OMI/MLS trends are in reasonable agreement, given some differences in data selection and minor differences in trend start and end dates: FT and TrCO ozone increases ∼+(2-8)%/decade. Likewise, the IASI/Metop trend for TrCO, (0.0±1.4)%/decade over 2008-2023 (Boynard et al., 2025) is an outlier over SE Asia.

Nowhere are the satellite data as divergent from the FT sonde trends, near zero change from our study (1998-2023), Gaudel et al. (2024, for 2004-2019) and HEGIFTOM-1 (2000-2022), than at Samoa (**Table 6**). TrCO from the SHADOZ sondes has no significant change: (-1.4 ±4.8)%/decade, this study); (-3.1±5.4)%/decade (Gaudel et al. 2024). However, the OMI/MLS trend for TrCO is (9.1±8.3)%/decade, 2005-2023, and IASI/Metop is (-9.0±1.7)%/decade (**Fig. 16a**). The large disagreement in trends from sondes and both satellite instruments, the latter with median TrCO trends that are offset by 18% from one another, underscore the need for profile-based tropospheric ozone trends as an unbiased reference.

### 4.3  **Implications of this study for TOAR II and related assessments**

How do our findings apply to an overall TOAR II assessment for tropical ozone? First, there is consensus among the four GB studies: this study, Gaudel et al (2024) and the two HEGIFTOM articles (HEGIFTOM-1; HEGIFTOM-2). These results provide well-characterized trends in FT ozone for input to climate models and a reference for evaluating TrCO, total tropospheric column ozone trends from evolving tropospheric ozone satellite products. In short, over the past 20-25 years, except for equatorial SE Asia, tropical FT and total tropospheric ozone trends are negligible to within ±(1-2)%/decade (**Fig. 9**). For SE Asia both FT and TrCO have increased from ∼(2-8)%/decade. Detailed analyses of sonde profiles by S24 suggest that the annually averaged FT ozone trends are (2-3)%/decade. The (5-7)%/decade increases are seasonal in FT ozone. However, for TrCO it is the large ozone increases in the boundary layer found throughout the year that are dominating the total tropospheric column change (**Fig. 11**).

Second, as far as methods of computing trends, we have shown both the similarity of median trends from QR and MLR as relative advantages of each with SHADOZ and combined SHADOZ-IAGOS profile data. HEGIFTOM-1 reached similar conclusions about QR and MLR trends for 34 ozonesonde stations, including 10 from SHADOZ. The complementarity of QR and MLR for trends attribution was also highlighted in HEGIFTOM-1. The HEGIFTOM papers (HEGIFTOM-1, HEGIFTOM-2), with a multi-instrument perspective, show variable trends among 55 global stations, including over western Europe and North America where both positive and negative tropospheric column trends occur within few

21

752 hundred km. Overall, except for southeast Asia, FT ozone trends from HEGIFTOM are small to moderate

753 and not distinguishable from zero at a number of tropical and extratropical locations. Third, both

754 HEGIFTOM-1 and this study investigated the matter of sample density in ground-based data, the former

755 by cutting sample size roughly in half for TrCO and our SHADOZ-IAGOS analyses for FT ozone, roughly

756 doubling it. In both studies trend changes determined with MLR were small (a few tenths of a

757 ppbv/decade) and included both increases and decreases (well-illustrated in Fig. S6 in HEGIFTOM-1).

758 Uncertainty changes ranged from 15-30%, usually improving with more sampling. We conclude that

759 arguments for excluding ground-based trends from TOAR II on the basis of sample size have little merit,

760 particularly given ongoing uncertainties and limited record lengths of many satellite products. Fourth,

761 by reducing the trend period from 26 years to 12 years, we quantified the degradation of too-short

762 trends for the relatively small changes that apply to much of global FT ozone.

763 The length of record is only one issue for ozone products derived from satellites that have operated

764 less than two decades. Trends based on the lowermost levels of ozone from MLS (Froidevaux et al.,

765 2025) were largely the same at all SHADOZ stations, (3-4%/decade for the UT, **Fig. 16c**) whereas the

766 sonde-derived trends are geographically variable. Only one of 5 tropical regions we analyzed, Atlantic

767 and western Africa, displayed a UT ozone trend in this range. The discrepancies between GB-based

768 trends are not surprising because MLS does not capture observed variability in UT ozone

769 concentrations, up to a factor of 2 between the Atlantic and eastern Indian Ocean, that is detected by the

770 sondes or UV sensors (Thompson et al., 2003; Thompson et al., 2017). We compared our profile-based

771 trends to two typical satellite products: IASI/Metop and the well-characterized OMI/MLS. Within the

772 uncertainty of the satellite trends, OMI/MLS TrCO trends agreed with TrCO$_{sonde}$ trends, but the largest

773 differences (positive trends versus negative trends respectively) were over the equatorial Americas and

774 Samoa. Where sonde-derived trends were near-zero, IASI/Metop trends sometimes agreed well but for

775 equatorial SE Asia the IASI/Metop zero trend clearly underestimated trends relative to those derived

776 from SHADOZ, SHADOZ-IAGOS combined profiles and OMI/MLS. At Samoa IASI/Metop (-9%/decade)

777 and OMI/MLS (+9%/decade) were both in error, displaying much greater disagreement with the sonde-

778 based trend than anywhere else. There is no easy explanation, but the differing wavelengths, vertical

779 sensitivities, and respective biases in the satellite products likely all play a role.

780 The S24 TOAR-II study is a reminder that the near-zero annually averaged FT ozone trends over most

781 of the tropics (**Figs. 8** and **13**) may mask strong seasonal trends (T21). S24 linked the strong February-

782 April increase in FT ozone over KL-Java (1998 to 2022) to declining convection with 4 proxies, e.g.,

783 outgoing long-wave radiation, velocity potential at 200 hPa. A role for changing dynamics must be

784 considered in tropical tropospheric ozone increases; increasing ozone precursor emissions are

785 apparently not the only driver. In a similar manner, decreases observed in LMS ozone appear to be

786 related to tropopause height changes during the 1998 to 2023 period.

22

787    In summary, our updated trends for SHADOZ stations (**Figs. 9** and **11**) remain the most reliable trend

788    reference throughout the tropical troposphere and LMS. We provide a definitive standard for evaluating

789    monthly trends and regional variability of satellite-based products and related models being used for

790    tropical trends in the past ~25 years. Together with the more extensive HEGIFTOM and IAGOS coverage,

791    our analyses lead to a conclusion that the most reliable trends for TOAR II are based on re-processed GB

792    measurements. However, coverage of the GB instruments is uneven and space-based observations are

793    needed for truly global trends. In order for satellite products to mature and for differences among them

794    to be understood, independent ozone data collection, particularly from ozonesondes referenced to an

795    absolute standard are required. As our investigations with the high-resolution SHADOZ profiles have

796    demonstrated, sonde data will remain the gold standard for deriving trends in the FT and LMS, the two

797    most critical regions where ozone interacts with the climate system.

798
799  **Data Availability**

800
801  All datasets used in this study are openly and publicly accessible.
802  V06 SHADOZ data are available at https://doi.org/10.57721/SHADOZ-V06 (NASA Goddard Space Flight Center
803  (GSFC) SHADOZ Team, 2019).
804  IAGOS and SHADOZ HEGIFTOM data are available at: https://hegiftom.meteo.be
805  Trends in table (*.csv) format are available at: https://tropo.gsfc.nasa.gov/shadoz/SHADOZ_PubsList
806  OMI/MLS data are available at https://acd-ext.gsfc.nasa.gov/Data_services/cloud_slice/new_data.html.

807

814
815  **Author Contributions**
816  Conceptualization of the study was by AMT, RMS, DEK. AMT led the writing with RMS and DEK, additional input
817  from GAM and KM. Analyses were carried out by RMS and DEK. All authors collected and/or contributed data.

818
819  **Editorial Input.** The article was handled by Editor E. Landulfo and benefitted from two anonymous reviewers.

820
821  **Competing Interests.** All authors declare that we have no competing interests.

822
823  **Acronyms and Chemical Names**

824
825  AIRS = Atmospheric Infrared Sounder
826  CAM-Chem = Community Atmosphere Model with Chemistry
827  $CH_4$ = Methane
828  DU = Dobson Units
829  ECC = Electrochemical Concentration Cell
830  ENSO = El Niño Southern Oscillation
831  FT = Free troposphere
832  FTIR = Fourier Transform Infrared
833  GAW = Global Atmospheric Watch
834  GB = Ground-based

835 HEGIFTOM = Harmonization and Evaluation of Ground-based Instruments for Free-Tropospheric Ozone
836     Measurements
837 IASI = Infrared Atmospheric Sounding Interferometer
838 IGAC = International Global Atmospheric Chemistry
839 IOD = Indian Ocean Dipole
840 ITCZ = Inter-Tropical Convergence Zone
841 KL = Kuala Lumpur
842 LMS = Lowermost stratosphere
843 MEI = Multivariate ENSO Index
844 MLR = Multi-linear Regression
845 MLS = Microwave Limb Sounder
846 NDACC = Network for the Detection of Atmospheric Composition Change
847 $O_3$ = Ozone
848 OH = Hydroxyl (radical)
849 OMI = Ozone Monitoring Instrument
850 QBO = Quasi-biennial Oscillation
851 QR = Quantile Regression
852 SC-Para = San Cristóbal-Paramaribo
853 SHADOZ = Southern Hemisphere Additional Ozonesondes
854 TOAR = Tropospheric Ozone Assessment Report
855 TH = Tropopause Height
856 TCO = Total Column Ozone
857 TrCO = Tropospheric Column Ozone (TrOC in HEGIFTOM)
858 TROPESS = TRopospheric Ozone and its Precursors from Earth System Sounding
859 UV = Ultraviolet
860 WAACM = Whole Atmosphere Community Climate Model
861 WMO = World Meteorological Organization
862
863 **References**
864

865 Aumann, H. H., Broberg, S., and Manning, E. M., Northward shift and narrowing of the ITCZ in 20 years of AIRS data,
866     J. Geophys. Res. Atmos. 129, e2023JD038723, https://doi.org/10.1029/2023JD038723, 2024.
867 Boynard, A., Wespes, C., Hadji-Lazaro, J., Sinnathamby, S., Hurtmans, D., Coheur, P-F., Doutriaux-Boucher, M.,
868     Onderwaater, J., Steinbrecht, W., Pennington, E. A., Bowman, K., and Clerbaux, C.: Tropospheric Ozone
869     Assessment Report (TOAR): 16-year ozone trends from the IASI climate data record,
870     https://doi.org/10.5194/egusphere-2025-1054, in review, 2025.
871 Cazorla, M.: Ozone structure over the equatorial Andes from balloon-borne observations and zonal connection with
872     two tropical seal level sites, *J. Atmos. Chem.,* 2016. https://doi.org/10.1007/s10874-016-9348-2
873 Cazorla, M., Parra, R., Herrera, E., and da Silva, F. R.: Characterizing ozone throughout the atmospheric column over the
874     tropical Andes from in situ and remote sensing observations. Elementa. 2021
875     https://doi.org/10.1525/elementa.2021.00019, 2021
876 Cazorla, M., and Herrera, E.: An ozonesonde evaluation of spaceborne observations in the Andean tropics. *Scientific*
877     *Reports* **12**, 15942. https://doi.org/10.1038/s41598-022-20303-7, 2022
878 Chang, K.-L., Cooper, O. R., Gaudel, A., Petropavlovskikh, I., and Thouret, V.: Statistical regularization for trend
879     detection: An integrated approach for detecting long-term trends from sparse tropospheric ozone profiles, Atmos.
880     Chem. Phys., 20, 9915-9938, https://doi.org/10.5194/acp-20-9915-2020, 2020
881 Chang, K.-L., Schultz, M.G., Lan, X., McClure-Begley, A., Petropavlovskikh, I., Xu, X., and Ziemke, J.R.: Trend detection of
882     atmospheric time series: Incorporating appropriate uncertainty estimates and handling extreme events. Elem Sci
883     Anth, 9(1), 00035, https://doi.org/10.1525/elementa.2021.00035, 2021.
884 Chang, K. L., Schultz, M. G., Koren, G., and Selke, N.: (2023). Guidance note on best statistical practices for TOAR
885     analyses. https://doi.org/10.48550/arXiv.2304.14236.
886 Christiansen, A., Mickley, L. J., Liu, J., Oman, L. D., and Hu, L.: Multidecadal increases in global tropospheric ozone
887     derived from ozonesonde and surface site observations: can models reproduce ozone trends? Atmos. Chem. Phys.,
888     https://doi.org/10.5194/acp-22-14751-2022, 2022.

889 Cooper, O. R., Schultz, M., G. Schröder, S., Chang, K.-L., Gaudel, A., Carbajal Benítez, G., Cuevas, E., Fröhlich, M., Galbally,
890   I. E., Kubistin, D., Lu, X., McClure-Begley, A., Molloy, S., Nédélec, P., O'Brien, J., Oltmans, S. J., Petropavlovskikh, I.,
891   Ries, L., Senik, I., Sjöberg, K., Solberg, S., Spain, T. G., Spangl, W., Steinbacher, M., Tarasick, D., Thouret, V., and Xu, X.:
892   Multi-decadal surface ozone trends at globally distributed remote locations, Elem Sci Anth, 8(1), p.23. DOI:
893   http://doi.org/10.1525/elementa.420,
894 De Mazière, M., Thompson, A. M., Kurylo, M. J., Wild, J. D., Bernhard, G., Blumenstock, T., Braathen, G. O., Hannigan, J. W.,
895   Lambert, J.-C., Leblanc, T., McGee, T. J., Nedoluha, G., Petropavlovskikh, I., Seckmeyer, G., Simon, P. C., Steinbrecht,
896   W., and Strahan, S. E.: The Network for the Detection of Atmospheric Composition Change (NDACC): history, status
897   and perspectives, Atmos. Chem. Phys., 18, 4935–4964, https://doi.org/10.5194/acp-18-4935-2018, 2018
898 Froidevaux, L., Kinnison, D. E., Gaubert, B., Schwartz, M. J., Livesey, N. J., Read, W. G., Bardeen, C. G., Ziemke, J. R., and
899   Fuller, R. A.: Tropical upper-tropospheric trends in ozone and carbon monoxide (2005–2020): observational and
900   model results, Atmos. Chem., Phys., https://doi.org/10.5194/acp-25-597-2025, 2025
901 Gaudel, A., Cooper, O. R., Ancellet, G., Barret, B., Boynard, A., Burrows, J. P., Clerbaux, C., Coheur, P.-F., Cuesta, J., Cuevas,
902   E., Doniki, S., Dufour, G., Ebojie, F., Foret, G., Garcia, O., Granados Muños, M. J., Hannigan, J. W., Hase, F., Huang, G.,
903   Hassler, B., Hurtmans, D., Jaffe, D., Jones, N., Kalabokas, P., Kerridge, B., Kulawik, S. S., Latter, B., Leblanc, T., Le
904   Flochmoën, E., Lin, W., Liu, J., Liu, X., Mahieu, E., McClure-Begley, A., Neu, J. L., Osman, M., Palm, M., Petetin, H.,
905   Petropavlovskikh, I., Querel, R., Rahpoe, N., Rozanov, A., Schultz, M. G., Schwab, J., Siddans, R., Smale, D.,
906   Steinbacher, M., Tanimoto, H., Tarasick, D. W., Thouret, V., Thompson, A. M., Trickl, T., Weatherhead, E., Wespes, C.,
907   Worden, H. M., Vigouroux, C., Xu, X., Zeng, G., and Ziemke, J.: Tropospheric Ozone Assessment Report: Present-day
908   distribution and trends of tropospheric ozone relevant to climate and global atmospheric chemistry model
909   evaluation, Elem. Sci. Anth., 6, 39, https://doi.org/10.1525/elementa.291, 2018.
910 Gaudel, A., Cooper, O. R., Chang, K-L., Bourgeois, I., Ziemke, J. R., Strode, S. A. Oman, L. D., Sellitto, P., Nedelec, P., Blot, R.,
911   Thouret, V., and Granier, C.: Aircraft observations since the 1990s reveal increases of tropospheric ozone at
912   multiple locations across the Northern Hemisphere, Science Advances, 6, (34), DOI: 10.1126/sciadv.aba8272, 2020
913 Gaudel, A. Bourgeois, I., Li, M., Chang, K.-L., Ziemke, J., Sauvage, R., Stauffer, R. M., Thompson, A. M., Kollonige, D. E.,
914   Smith, N., Hubert, D., Keppens, A., Cuesta, J., Heue, K.-P., Veefkind, P., Aikin, K., Peischl, J., Thompson, C. R., Ryerson,
915   T. B., Frost, G. J., McDonald, B. C., and Cooper, O. R.: Tropical tropospheric ozone distribution and trends from in
916   situ and satellite data, Atmos. Chem. Phys., https://acp.copernicus.org/articles/24/9975/2024, 2024
917   Godin-Beekmann, S., Azouz, N., Sofieva, V. F., Hubert, D., Petropavlovskikh, I., Effertz, P., Ancellet, G., Degenstein, D. A.,
918   Zawada, D., Froidevaux, L., Frith, S., Wild, J., Davis, S., Steinbrecht, W., Leblanc, T., Querel, R., Tourpali, K.,
919   Damadeo, R., Maillard Barras, E., Stübi, R., Vigouroux, C., Arosio, C., Nedoluha, G., Boyd, I., Van Malderen, R.,
920   Mahieu, E., Smale, D., and Sussmann, R.: Updated trends of the stratospheric ozone vertical distribution in the
921   60° S–60° N latitude range based on the LOTUS regression model , Atmos. Chem. Phys., 22, 11657–11673,
922   https://doi.org/10.5194/acp-22-11657-2022, 2022.
923   Keppens, A., Hubert, D., Granville, J., Nath, O., Lambert, J.-L., Wespes, C., Coheur, P.-F., Clerbaux, C., Boynard, A.,
924   Siddans, R., Latter, B., Kerridge, B., Di Pede, S., Veefkind, P., Cuesta, J., Dufour, G., Heue, K.-P., Coldewey-Egbers, M.,
925   Loyola, D., Orfanoz-Cheuquelaf, A., Satheesan, S. M., Eichmann, K.-U., Rozanov, A., Sofieva, V. F., Ziemke, J. R.,
926   Inness, A., Van Malderen, R., and Hoffmann, L., Harmonisation of sixteen tropospheric ozone satellite data
927   records, egusphere-2024-3746, in review, 2025
928   Khalil, M. A. K., Atmospheric Methane: Its Role in the Global Environment, Springer-Verlag, Berlin, Heidelberg,
929   https://doi.org/10.1007/978-3-662-04145-1, 2000.
930   Koenker, R. (2005). Quantile regression, vol. 38, Cambridge University press,
931   https://doi.org/10.1017/CBO9780511754098
932   Lacis, A. A. Wuebbles, D. J., and Logan, J. A., Radiative forcing of climate by changes in the vertical distribution of
933   ozone, , J. Geophys. Res. Atmos. 101, 9971-9982, https://doi.org/10.1029/JD095iD07p09971, 1990
934 Lee, S., Shelow, D. M., Thompson, A. M., and Miller, S. K.: QBO and ENSO variability in temperature and ozone from
935   SHADOZ (1998-2005), J. Geophys. Res. Atmos., 115, D18105, doi: 10.1029/2009JD013320, 2010
936 Millet, T., Bencherif, H., Bègue, N., Portafaix, T., Toihir, A. M., Sivakumar, V., Vaz Peres, L., Fontaine, M., Pazmiño, A.,
937   Metzger, J-M., Stauffer, R. M., Kollonige, D. E., Thompson, A. M., Evidence for subtropical dynamical changes in
938   Réunion ozone trends (1998-2021), https://essopenarchive.org/users/664913/articles/1287997, 2025
939 Müller, K., Tradowsky, J. S., von der Gathen, P., Ritter, C., Patris, S., Notholt, J., Rex, M.: Measurement report: The Palau
940   Atmospheric Observatory and its ozonesonde record – continuous monitoring of tropospheric composition and
941   dynamics in the tropical western Pacific, Atmos. Chem. Phys., 24, 2169–2193, https://doi.org/10.5194/ acp-24-
942   2169-2024, 2024
943 Nakano, T., and Morofuji, T.:Development of an automated pump-efficiency measuring system for ozonesondes
944   utilizing an airbag-type flowmeter, Atmos. Meas. Tech., 16, 1583–1595, https://doi.org/10.5194/ amt-16-1583-
945   2023, 2023

946 NASA Goddard Space Flight Center (GSFC) SHADOZ Team: Southern Hemisphere ADditional OZonesondes (SHADOZ)
947     Version 06 (V06) Station Data (Version V06), NASA [data set], https://doi.org/10.57721/SHADOZ-V06, 2019
948 Pennington, E. A., Osterman, G. B., Payne, V. H., Miyazaki, K., Bowman, K. W., and Neu, J. L.: Quantifying biases in
949     TROPESS AIRS, CrIS, and joint AIRS+OMI tropospheric ozone products using ozonesondes,
950     https://doi.org/10.5194/ egusphere-2024-3701, in review, 2025
951 Plumb, A. R.: A "tropical pipe" model of stratospheric transport, J. Geophys. Res. Atmos. 101 (D6), 3957-3972,
952     https://doi.org/10.1029/95JD03002, 1996
953 Pope, R. J., Kerridge, B. J., Siddans, R., Latter, B. G., Chipperfield, M. P., Feng, W., Pimlott, M. A., Dhomse, S. S., Retscher,
954     C., and Rigby, R.: Investigation of spatial and temporal variability in lower tropospheric ozone from RAL Space UV–
955     Vis satellite products, Atmos. Chem. Phys., 23, 14933–14947, https://doi.org/10.5194/acp-23-14933-2023, 2023
956 Randel, W. J., Park, M., and Wu, F.: A large annual cycle in ozone above the tropical tropopause linked to the Brewer–
957     Dobson circulation, J. Atmos. Sci., 64, 4479-4488, doi: 10.1175/2007JAS2409.1, 2007
958 Randel, W. J., and Thompson, A. M.: Interannual variability and trends in tropical ozone derived from SHADOZ
959     ozonesondes and SAGE II satellite data, J. Geophys. Res. Atmos., 116, D07303, doi:10.1029/ 2010JD015195, 2011
960 Schwartzkopf, M. D., and Ramaswamy, V., Radiative forcing due to ozone in the 1980s: Dependence on altitude of
961     ozone change, Geophysical Res. Letters, https://doi.org/10.1029/93GL00209, 1993
962 Smit, H. G. J., Poyraz, D., Van Malderen, R., Thompson, A. M., Tarasick, D. W., Stauffer, R. M., Johnson, B. J., and Kollonige,
963     D. E., New insights from the Jülich Ozone-Sonde Intercomparison Experiments: Calibration functions traceable to
964     one ozone reference instrument, Atmos. Meas. Tech., 17, 73–112, https://doi.org/10.5194/amt-17-73-2024, 2024
965 Smit, H. G. J., Galle, T., Blot, R., Obersteiner, F., Nédélec, P., Zahn, A., Cousin, J-M., Bundke, U., Petzold, A., Thouret, V., and
966     Clark, H., Intercomparison of IAGOS-CORE, IAGOS-CARIBIC and WMO/GAW-WCCOS ozone instruments at the
967     Environmental Simulation Facility at Jülich, Germany, https://doi.org/10.5194/egusphere-2024-3760, 2025
968 Stauffer, R. M., Thompson, A. M., and Witte, J. C.: Characterizing global ozonesonde profile variability from surface to
969     the UT/LS with a clustering technique and MERRA-2 reanalysis, J. Geophys. Res. Atmos., 123, 6213–6229,
970     https://doi.org/10.1029/2018JD028465, 2018
971 Stauffer, R. M., Thompson, A. M., Kollonige, D. E., Witte, J. C., Tarasick, D. W., Davies, J., Vömel, H., Morris, G. A., van
972     Malderen, R., Johnson, B. J., Querel, R. R., Selkirk, H. B., Stübi, R., and Smit, H. G. J.: A post-2013 dropoff in total ozone
973     at a third of global ozonesonde stations: Electrochemical concentration cell instrument artifacts? Geophys. Res.
974     Lett., 47, e2019GL086791. https://doi.org/10.1029/2019GL086791, 2020
975  Stauffer, R. M., Thompson, A. M., Kollonige, D. E., Tarasick, D. W., Van Malderen, R., Smit, H. G. J., Vömel, H., Morris, G.
976     A., Johnson, B. J., Cullis, P. D., Stübi, R., Davies, J., and Yan, M. M.: An examination of the recent stability of
977     ozonesonde global network data, *Earth Space. Sci.,* https://doi.org/10.1029/2022EA002459, 2022
978  Stauffer, R. M., Thompson, A. M., Kollonige, D. E., Komala, N., Khirzin Al-Ghazali, H., Risdianto, D. Y.,Dindang, A., bin
979     Jamaluddin, A. F., Sammathuria, M. K., Zakaria, N. B., Johnson, B. J., and Cullis, P. D., Dynamical drivers of free-
980     tropospheric ozone increases over equatorial Southeast Asia, Atmos. Chem. Phys.,
981     https://doi.org/10.5194/acp-24-5221-2024, 2024
982 Stolarski, R. S., Bloomfield, P. R., McPeters, R. D., and Herman, J. R.: Total ozone trends deduced from Nimbus 7 TOMS
983     data, Geophys. Res. Lett., 18, 1015-1018, https://doi.org/10.1029/91GL01302, 1991
984 Thompson, A. M.: The oxidizing capacity of the Earth's atmosphere: Probably past and future changes, Science,
985     https://doi.org/10.1126/science.256.5060.1157, 1992
986 Thompson, A. M., and Cicerone, R. J.: Atmospheric $CH_4$, CO, and OH from 1860 1985, Nature, 321, 148 150;
987     https://www.nature.com/articles/321148a0, 1986
988 Thompson, A. M., Huntley, M. A., and Stewart, R. W.: Perturbations to tropospheric oxidants, 1985-2035: 1. Model
989     calculations of ozone and OH in chemically coherent regions, J. Geophys. Res. Atmos.,
990     https://doi.org/10.1029/JD095iD07p09829, 1990
991 Thompson, A. M., Witte, J. C., Hudson, R. D., Guo, H., Herman, J. R., and Fujiwara, M.: Tropical tropospheric ozone and
992     biomass burning, *Science,* 291, 2128-2132, 2001; doi: 10.1126/science.291.5511.2128
993 Thompson, A. M., Witte, J. C., , Oltmans, S. J., Schmidlin, F. J, Logan, J. A., Fujiwara, M., Kirchhoff, V. W. J. H., Posny, F.,
994     Coetzee, G. J. R., Hoegger, B., Kawakami, S., Ogawa, T., Fortuin, J. P. F., and Kelder, H.: Southern Hemisphere
995     ADditional Ozonesondes (SHADOZ) 1998-2000 tropical ozone climatology. 2. Tropospheric variability and the
996     zonal wave-one, J. Geophys. Res. Atmos., 108, 8241, doi: 10.1029/2002JD002241, 2003
997 Thompson, A. M., Witte, J. C., Smit, H. G. J., Oltmans, S. J., Johnson, B. J., Kirchhoff, V. W. J. H., and Schmidlin, F. J.:
998     Southern Hemisphere Additional Ozonesondes (SHADOZ) 1998-2004 tropical ozone climatology. 3.
999     Instrumentation, Station Variability, Evaluation with Simulated Flight Profiles, J. Geophys. Res., 112, D03304, doi:
1000     10.1029/ 2005JD007042, 2007

1001 Thompson, A. M., Allen, A. L., Lee, S,. Miller, S. K., and Witte, J. C.: Gravity and Rossby wave signatures in the tropical
1002     troposphere and lower stratosphere based on Southern Hemisphere Additional Ozonesondes (SHADOZ), 1998–
1003     2007, *J. Geophys. Res. Atmos.,* 116, D05302, doi:10.1029/2009JD013429, 2011
1004 Thompson, A. M., Miller, S. K., Tilmes, S., Kollonige, D. W., Witte, J. C., Oltmans, S. J., Johnson, B. J., Fujiwara, M.,
1005     Schmidlin, F. J., Coetzee, G. J. R., Komala, N., Maata, M.. bt Mohamad, M., Nguyo, J., Mutai, C., Ogino, S.-Y., Raimundo
1006     Da Silva, F., Paes Leme, N. M., Posny, Scheele, R., F. Selkirk, H. B., Shiotani, M., Stübi, R., Levrat, G., Calpini, B.,
1007     Thouret, V., Tsuruta, H., Valverde Canossa, J. Vömel, H., Yonemura, S. Andrés Diaz, J., Tan Thanh, N, T., and Thuy Ha,
1008     H. T.: Southern Hemisphere Additional Ozonesondes (SHADOZ) ozone climatology (2005-2009): Tropospheric and
1009     tropical tropopause layer (TTL) profiles with comparisons to OMI-based ozone products. J. Geophys. Res., **117,**
1010     D23301, doi: 10.1029/2010JD016911, 2012
1011 Thompson, A. M., Balashov, N.V., Witte, J. C., Coetzee, G. J. R., Thouret, V., and Posny, F.: Tropospheric ozone increases
1012     in the southern African region: Bellwether for rapid growth in southern hemisphere pollution?  Atmos. Chem.
1013     Phys., **14,** 9855-9869, 2014.
1014 Thompson, A. M., Witte, J. C., Sterling, C., Jordan, A., Johnson, B. J., Oltmans, S. J., Fujiwara, M., Vömel, H., Allaart, M.,
1015     Piters, A., Coetzee, G. J. R., Posny, F., Corrales, E., Andres Diaz, J., Félix, C. Komala, N., Lai N., Maata, M., Mani, F.,
1016     Zainal, Z., Ogino, S.-Y., Paredes, F., Luiz Bezerra Penha, T., Raimundo da Silva, F., Sallons-Mitro, F., Selkirk, H. B.,
1017     Schmidlin, F. B., Stuebi, R., and Thiongo, K.: First reprocessing of Southern Hemisphere Additional Ozonesondes
1018     (SHADOZ) ozone profiles (1998–2016): 2. Comparisons with satellites and ground-based instruments, J. Geophys.
1019     Res. Atmos., 122, 13,000–13,025, 2017; https://doi.org/10.1002/2017JD027406
1020 Thompson, A. M., Smit, H. G. J., Witte, J. C., Stauffer, R. M., Johnson, B. J., Morris, G. A., von der Gathen, P., Van Malderen,
1021     R., Davies, J., Piters, A., Allaart, M., Posny, F., Kivi, R., Cullis, P., Ahn, N. T. H., Corrales, E., Machinini, T., Raimundo
1022     daSilva, F., Paiman, G., Thiong'o, K., Zainal, Z., Brothers, G. B., Wolff, K. R., Nakano, T., Stübi, R., Romanens, G.,
1023     Coetzee, G. J. R., Diaz, J. A., Mitro, S., 'bt Mohamad, M., and Ogino, S.-Y.: Ozonesonde Quality Assurance: The JOSIE-
1024     SHADOZ (2017) Experience, Bull. Am. Meteor. Society, doi.org/10.1175/BAMS-17-0311, 2019
1025  Thompson, A. M., Stauffer, R. M., Wargan, K., Witte, J. C., Kollonige, D. E., and Ziemke, J. R.: Regional and seasonal
1026     trends in tropical ozone from SHADOZ profiles: Reference for models and satellite products, J. Geophys. Res
1027     Atmos., https://agupubs.onlinelibrary.wiley.com/doi/10.1029/2021JD034691, 2021
1028  Thouret, V., Clark, H., Petzold, A., Nédélec, P., and Zahn, A.:. IAGOS: Monitoring Atmospheric Composition for Air
1029     Quality and Climate by Passenger Aircraft. (pp. 1-14). https://doi.org/10.1007/978-981-15-2527-8_57-1, 2022
1030  Tselioudis, G., Remillard, J., Jakob, C.,  and Rossow, W. B.: Contraction of the world's storm-cloud zones the primary
1031     contributor to the 21st century increase in the Earth's sunlight absorption. Geophys. Res., Lett.,
1032     https://doi.org/10.1029/2025GL114882, 2025
1033  Tsivlidou, M., Sauvage, B., Bennouna, Y., Blot, R., Boulanger, D., Clark, H., Le Flochmoën, E., Nédélec, P., Thouret, V.,
1034     Wolff, P. & Barret, B.: Tropical tropospheric ozone and carbon monoxide distributions: characteristics, origins,
1035     and control factors, as seen by IAGOS and IASI. (Vol. 23, pp. 14039-14063). https://doi.org/10.5194/acp-23-
1036     14039-2023, 2023
1037 Van Malderen, R., Thompson, A. M., Kollonige, D. E., Stauffer, R. M., Smit, H. G. J., Maillard Barras, E., Vigouroux, C.,
1038     Petropavlovskikh, I., Leblanc, T.. Thouret, V., Wolff, P., Effertz, P., Tarasick, D. W., Poyraz, D., Ancellet, G., De Backer,
1039     M.-R., Evan, S., Flood, V., Frey, M. M., Hannigan, J. W., Hernandez, J. L., Iarlori, M., Johnson, B. J., Jones, N., Kivi, R.,
1040     Mahieu, E., McConville, G., Müller, K., Nagahama, T., Notholt, J.,  Piters, A., Prats, N., Querel, R., Smale, D., Steinbrecht,
1041     W., Strong, K., and Sussmann, R.: Global ground-based tropospheric ozone measurements: Reference data and
1042     individual site trends (2000–2022) from the TOAR-II/HEGIFTOM Project, Atmos. Chem. Phys. 25, 7187–7225,
1043     https://doi.org/10.5194/acp-25-7187-2025, 2025a
1044 Van Malderen, R., Zang, Z., Chang, K.-L., Björklund, R., Cooper, O. R., Liu, J., Barras, E. M., Vigouroux, C.,
1045     Petropavlovskikh, I., Leblanc, T., Thouret, V., Wolff, P., Effertz, P., Gaudel, A., Tarasick, D. W., Smit, H. G. J.,
1046     Thompson, A. M., Stauffer, R. M., Kollonige, D. E., Poyraz, D., Ancellet, G., De Backer, M.-R., Frey, M. M., Hannigan, J.
1047     W., Hernandez, J. L., Johnson, B. J., Jones, N., Kivi, R., Mahieu, E., Morino, I., McConville, G., Müller, G., Murata, I.,
1048     Notholt, J., Piters, A., Prignon, M., Querel, R., Rizi, V., Smale, D., Steinbrecht, W., Strong, K., and Sussmann, R.: Global
1049     ground-based tropospheric ozone measurements: Regional tropospheric ozone column trends from the TOAR-
1050     II/HEGIFTOM homogenized datasets, Atmos. Chem., Phys., DOI: 10.5194/egusphere-2024-3745, in press, 2025b
1051 Wargan, K., Orbe, C., Pawson, S., Ziemke, J. R., Oman, L. D., Olsen, M. A., Coy, L., and Knowland, K. E., Recent decline in
1052     extratropical lower stratospheric ozone attributed to circulation changes, Geophysical Research Letters,
1053     https://doi.org/10.1029/2018GL077406, 2018
1054 Wilks, D.S. (1997). Resampling hypothesis tests for autocorrelated fields, J. Climate, 10 (1), 65-82,
1055     https://doi.org/10.1175/1520-0442(1997)010<0065:RHTFAF>2.0.CO;2
1056 Witte, J. C., Thompson, A. M., Smit, H. G. J., Fujiwara, M., Posny, F., Coetzee, G. J. R., Northam, E. T., Johnson, B. J.,
1057     Sterling, C. W., Mohammed, M., Ogino, S.-Y., Jordan, A., Raimundo Silva, F., and Zainal, Z.: First reprocessing of

1058     Southern Hemisphere ADditional OZonesondes (SHADOZ) profile records (1998-2015) 1: Methodology and
1059     evaluation, J. Geophys. Res., 122, 6611-6636, doi: 10.1002/2016JD026403, 2017
1060 Zhang, Y., Cooper, O. R., Gaudel, A., Thompson, A. M., Nédelec, P., Ogino, S.-Y., and West, J. J.: Equatorward
1061     redistribution of emissions dominates the 1980 to 2010 tropospheric ozone change, Nature-Geoscience, doi:
1062     10.1038/NGEO2827, 2016
1063 Ziemke, J. R., and Chandra, S.: Madden-Julian Oscillation in tropospheric ozone, J. Geophys. Res. Atmos.,
1064     https://doi.org/10.1029/2003GL018523, 2003
1065 Ziemke, J. R., Chandra, S., Duncan, B. N., Froidevaux, L., Bhartia, P. K., Levelt, P. F., and Waters, J. W.: Tropospheric
1066     ozone determined from Aura OMI and MLS: Evaluation of measurements and comparison with the Global
1067     Modeling Initiative's Chemical Transport Model, J. Geophys. Res., 111, D19303,
1068     https://doi.org/10.1029/2006JD007089, 2006
1069 Ziemke, J. R., Oman, L. D., Strode, S. A., Douglass, A. R., Olsen, M. A., McPeters, R. D., Bhartia, P. K., L. Froidevaux, L..
1070     Labow, G. J.,. Witte, J. C., Thompson, A. M., D. P. Haffner, D. P., Kramarova, N. A., Frith, S. M., Huang, L. K., Jaross, G. R.,
1071     Seftor, C. J., Deland, M. T., Taylor, S. L.: Trends in global tropospheric ozone Inferred from a composite record of
1072     TOMS/OMI/MLS/OMPS satellite measurements and the MERRA-2 GMI simulation, Atmos. Chem. Phys., 19, 3257–
1073     3269, 2019. https://doi.org/10.5194/acp-19-3257-2019, 2019
1074 Ziemke, J. R,, Kramarova, N. A., Frith, S. M., Huang, L. K., Haffner, D., Wargan, K.,, Lamsal, L. N., Labow, G. J., Bhartia, P. K.:
1075     NASA Satellite Measurements Show Global-Scale Reductions in Free Tropospheric Ozone in 2020 and Again in
1076     2021 During COVID-19, Geophys. Res., Lett. https://doi.org/10.1029/2022GL098712, 2022
1077

## Tables and Figures

**Table 1.** List of the 27 total SHADOZ and IAGOS sites, and their metadata, used in this analysis.

| Site | Country | Observation Network | Latitude | Longitude | Altitude (m) |
|---|---|---|---|---|---|
| Abidjan (ABJ) | Cote d'Ivoire | IAGOS | 5.25 | -3.93 | 6 |
| Accra (ACC) | Ghana | IAGOS | 5.61 | -0.17 | 62 |
| Addis Ababa (ADD) | Ethiopia | IAGOS | 8.98 | 38.80 | 2326 |
| *Ascension Island* | United Kingdom | SHADOZ | -7.58 | -14.24 | 85 |
| Bogota (BOG) | Colombia | IAGOS | 4.70 | -74.14 | 2548 |
| Brazzaville (BZV) | Congo (Brazzaville) | IAGOS | -4.26 | 15.25 | 319 |
| Caracas (CCS) | Venezuela | IAGOS | 10.60 | -67.01 | 71 |
| Cotonou (COO) | Benin | IAGOS | 6.35 | 2.39 | 6 |
| Douala (DLA) | Cameroon | IAGOS | 4.01 | 9.72 | 10 |
| *Hanoi* | Vietnam | SHADOZ | 21.01 | 105.80 | 6 |
| *Hilo, Hawaii* | United States | SHADOZ | 19.43 | -155.04 | 11 |
| *Irene* | South Africa | SHADOZ | -25.90 | 28.22 | 1524 |
| Kinshasa (FIH) | Congo (Kinshasa) | IAGOS | -4.39 | 15.45 | 313 |
| *Koror* | Palau | SHADOZ | 7.34 | 134.47 | 23 |
| *Kuala Lumpur* | Malaysia | SHADOZ | 2.73 | 101.27 | 17 |
| Kuala Lumpur (KUL) | Malaysia | IAGOS | 2.76 | 101.71 | 21 |
| Lagos (LOS) | Nigeria | IAGOS | 6.58 | 3.32 | 41 |
| Libreville (LBV) | Gabon | IAGOS | 0.46 | 9.41 | 12 |
| Lome (LFW) | Togo | IAGOS | 6.17 | 1.25 | 22 |
| Luanda (LAD) | Angola | IAGOS | -8.85 | 13.23 | 74 |
| Malabo (SSG) | Equatorial Guinea | IAGOS | 3.76 | 8.72 | 23 |
| *Nairobi* | Kenya | SHADOZ | -1.27 | 36.80 | 1795 |
| *Natal* | Brazil | SHADOZ | -5.42 | -35.38 | 42 |
| *Pago Pago* | American Samoa | SHADOZ | -14.23 | -170.56 | 77 |
| *Paramaribo* | Surinam | SHADOZ | 5.80 | -55.21 | 23 |
| Port Harcourt (PHC) | Nigeria | IAGOS | 5.01 | 6.95 | 27 |
| *Quito* | Ecuador | SHADOZ | -0.20 | -78.44 | 2414 |
| *Reunion Island* | France | SHADOZ | -21.06 | 55.48 | 10 |
| *San Cristobal* | Ecuador | SHADOZ | -0.89 | -89.61 | 8 |
| Sao Paulo (GRU) | Brazil | IAGOS | -23.43 | -46.48 | 750 |
| Singapore (SIN) | Singapore | IAGOS | 1.36 | 103.99 | 7 |
| *Suva* | Fiji | SHADOZ | -18.13 | 178.40 | 6 |
| *Watukosek, Java* | Indonesia | SHADOZ | -7.46 | 112.43 | 50 |
| Yaounde (NSI) | Cameroon | IAGOS | 3.70 | 11.55 | 694 |

Table 2. SHADOZ metadata: number of profiles, annual trends. Each row indicates a different segment: 5-10km, 10-15km, 15-20km, TH-5km to TH, TH to TH +5km, and surface to Tp (tropopause). Periods analyzed (columns) are 1998-2019 (T21), 1998-2023, 2000-2023; 2005-2023 for OMI/MLR comparisons in total tropospheric ozone column amount (TrCO). Annually-averaged MLR partial column ozone linear trends are shown DU per decade and in percent per decade, with the 95% confidence interval. Trends with p-values <0.05 are shown in bold.

| SHADOZ T21 Updated MLR FT Ozone Trends | | | | | | | | | | |
|---|---|---|---|---|---|---|---|---|---|---|
| Station | Altitude Range | Number of Profiles | 1998-2019 T21 Annual Trend ± 2*sigma (DU/decade) | 1998-2019 T21 Annual Trend ± 2*sigma (%/decade) | 1998-2023 Annual Trend ± 2*sigma (DU/decade) | 1998-2023 Annual Trend ± 2*sigma (%/decade) | 2000-2023 Annual Trend ± 2*sigma (DU/decade) | 2000-2023 Annual Trend ± 2*sigma (%/decade) | 2005-2023 Annual Trend ± 2*sigma (DU/decade) | 2005-2023 Annual Trend ± 2*sigma (%/decade) |
| San Cristobal – Paramaribo | 5-10km | 1370 | 0.2±0.3 | 1.9±3.1 | -0.1±0.3 | -0.9±3.7 | -0.1±0.3 | -1.2±3.8 | -0.3±0.5 | -3.6±5.1 |
| | 10-15km | | 0.1±0.2 | 1.5±4.0 | -0.2±0.3 | -3.5±4.5 | -0.2±0.3 | -4.0±4.4 | **-0.4±0.4** | **-6.6±6.5** |
| | 15-20km | | **-0.4±0.4** | **-3.1±2.8** | **-0.5±0.4** | **-3.9±2.9** | -0.4±0.4 | -2.8±3.2 | -0.4±0.7 | -3.3±5.5 |
| | TH-5km to TH | | 0.0±0.2 | 0.2±4.2 | -0.2±0.3 | -2.9±5.1 | -0.2±0.3 | -2.9±5.2 | -0.3±0.4 | -5.9±7.5 |
| | TH to TH+5km | | 0.2±0.6 | 0.6±2.3 | -0.3±0.7 | -1.2±2.6 | -0.3±0.8 | -1.1±2.9 | -0.4±1.3 | -1.5±4.5 |
| | TrCO, surf-Tp | | NA | NA | -0.3±0.9 | -1.0±3.3 | -0.2±1.0 | -0.8±3.6 | -0.4±1.6 | -1.4±5.9 |
| Natal - Ascension Island | 5-10km | 1646 | 0.2±0.3 | 1.6±2.3 | 0.2±0.3 | 1.9±2.2 | 0.1±0.2 | 0.5±1.8 | 0.0±0.4 | 0.3±2.9 |
| | 10-15km | | **0.3±0.2** | **3.9±2.8** | **0.2±0.2** | **3.4±2.9** | 0.1±0.2 | 1.7±2.4 | 0.1±0.3 | 0.7±3.8 |
| | 15-20km | | -0.0±0.3 | -0.4±2.4 | -0.1±0.3 | -1.0±2.3 | -0.2±0.3 | -1.4±2.6 | -0.3±0.5 | -2.4±3.8 |
| | TH-5km to TH | | **0.3±0.2** | **4.7±2.7** | **0.2±0.2** | **3.4±2.9** | 0.1±0.2 | 1.7±2.4 | 0.0±0.2 | 0.2±3.3 |
| | TH to TH+5km | | 0.5±0.5 | 1.9±1.9 | 0.2±0.7 | 0.9±2.7 | -0.0±0.6 | -0.1±2.5 | -0.4±0.9 | -1.6±3.7 |
| | TrCO surf-Tp | | NA | NA | **0.7±0.6** | **1.9±1.8** | 0.3±0.7 | 0.9±1.9 | 0.3±1.0 | 1.0±2.8 |
| Nairobi | 5-10km | 976 | 0.1±0.3 | 1.2±3.1 | 0.1±0.3 | 0.5±3.0 | 0.1±0.4 | 1.0±3.5 | -0.0±0.7 | -0.3±6.3 |
| | 10-15km | | -0.0±0.2 | -0.2±3.4 | -0.1±0.2 | -1.5±3.2 | -0.1±0.3 | -1.9±4.2 | -0.2±0.6 | -2.4±8.2 |
| | 15-20km | | 0.1±0.3 | 0.6±2.5 | 0.1±0.5 | 0.9±3.9 | 0.3±0.5 | 2.4±4.2 | 0.7±0.9 | 5.6±6.9 |
| | TH-5km to TH | | 0.0±0.2 | 0.7±3.2 | -0.0±0.2 | -0.0±2.5 | -0.0±0.2 | -0.1±3.3 | -0.0±0.4 | -0.2±6.1 |
| | TH to TH+5km | | 0.5±0.7 | 1.9±2.7 | 0.4±0.9 | 1.4±3.5 | 0.5±1.1 | 1.7±4.2 | 1.2±1.7 | 4.5±6.3 |
| | TrCO, Surf-Tp | | NA | NA | 0.3±0.7 | 1.1±2.5 | 0.3±0.9 | 1.0±3.2 | -0.4±1.5 | -1.5±5.2 |
| Kuala Lumpur – Watukosek | 5-10km | 870 | 0.1±0.2 | 1.9±3.0 | 0.1±0.2 | 1.0±2.5 | 0.1±0.2 | 1.0±3.1 | -0.1±0.3 | -1.2±4.3 |
| | 10-15km | | -0.0±0.1 | -0.6±3.3 | 0.0±0.1 | 1.3±3.6 | 0.1±0.2 | 2.9±4.2 | 0.2±0.2 | 4.3±6.6 |
| | 15-20km | | **-0.7±0.3** | **-5.8±2.8** | -0.3±0.6 | -2.4±4.8 | -0.1±0.6 | -0.4±5.3 | 0.6±0.8 | 5.2±6.8 |
| | TH-5km to TH | | -0.1±0.1 | -3.2±3.3 | 0.0±0.2 | 0.8±5.7 | 0.1±0.2 | 2.6±6.8 | 0.2±0.3 | 5.1±8.8 |

30

| | TH to TH+5km | | -0.1±0.8 | -0.5±3.0 | 0.2±1.1 | 0.9±4.2 | 0.3±1.2 | 1.1±4.5 | **1.7±1.0** | **7.0±4.0** |
|---|---|---|---|---|---|---|---|---|---|---|
| | TrCO, surf-Tp | | NA | NA | **0.6±0.6** | **2.6±2.3** | **1.1±0.7** | **4.6±2.8** | 0.7±1.1 | 3.0±4.6 |
| Samoa | 5-10km | 928 | 0.1±0.3 | 1.4±4.7 | 0.1±0.3 | 0.8±4.4 | -0.0±0.3 | -0.2±4.5 | -0.2±0.4 | -3.0±5.7 |
| | 10-15km | | 0.1±0.3 | 2.5±6.5 | -0.0±0.4 | -1.3±9.2 | -0.1±0.4 | -3.0±9.4 | **-0.4±0.4** | **-10.0±10.0** |
| | 15-20km | | -0.4±0.5 | -2.8±3.4 | -0.3±0.7 | -2.3±5.2 | -0.4±0.7 | -2.9±5.3 | **-1.0±0.8** | **-7.0±5.4** |
| | TH-5km to TH | | 0.0±0.3 | 0.2±6.5 | -0.1±0.4 | -1.7±8.8 | -0.1±0.4 | -2.5±9.5 | **-0.5±0.4** | **-10.6±9.0** |
| | TH to TH+5km | | -0.3±0.7 | -0.9±2.4 | -0.4±0.9 | -1.4±3.1 | -0.9±0.9 | -2.9±3.0 | **-1.2±1.1** | **-3.9±3.7** |
| | TrCO, surf-Tp | | NA | NA | -0.3±1.0 | -1.4±4.8 | -0.3±1.1 | -1.3±5.4 | -0.9±1.4 | -4.4±6.5 |

1088

**Table 3.** SHADOZ and IAGOS combined MLR ozone trends values for FTp (700-300 hPa) partial column for 5 regions: Equatorial Americas, Atlantic and West Africa, East Africa, Equatorial Southeast Asia, and Samoa (individual record). The individual sites are listed for each region. Annually-averaged MLR partial column ozone linear trends are shown DU per decade and in percent per decade, with the 95% confidence interval. Trends with p-values <0.05 are shown in bold.

| SHADOZ MLR Regional FT (700-300 hPa) Ozone Trends | | | | |
|---|---|---|---|---|
| **Region Name** | **Individual SHADOZ & IAGOS Locations (IAGOS regions in bold)** | **Number of Profiles** | **1998-2023 Annual Trend ± 2*sigma (DU/decade)** | **1998-2023 Annual Trend ± 2*sigma (%/decade)** |
| Equatorial Americas | San Cristobal (Ecuador), Paramaribo (Suriname), Quito (Ecuador), Caracas (Venezuela), Bogota (Colombia) | 2821 | 0.00 ± 0.31 | -0.01 ± 2.57 |
| Atlantic and West Africa | Natal (Brazil), Ascension Island (UK); **Central Africa** [Luanda (Angola), Brazzaville (Congo), Kinshasa (Democratic Republic of Congo)], **Gulf of Guinea** [ Lomé (Togo), Yaoundé (Cameroon), Douala (Cameroon), Libreville (Gabon), Accra (Ghana), Abidjan (Ivory Coast), Malabo (Equatorial Guinea), Cotonou (Benin), Port Harcourt (Nigeria)], **Lagos** (Nigeria) | 4271 | 0.12 ± 0.39 | 0.69 ± 2.28 |
| East Africa | Nairobi (Kenya), Addis Ababa (Ethiopia) | 1297 | 0.12 ± 0.38 | 0.85 ± 2.69 |
| Equatorial Southeast Asia | Kuala Lumpur (Malaysia), Watukosek (Indonesia); **Gulf of Thailand** [Kuala Lumpur (Malaysia), Singapore (Singapore)] | 1305 | 0.16 ± 0.34 | 1.57 ± 3.25 |
| Samoa | Pago Pago (Am. Samoa) | 928 | -0.04 ± 0.38 | -0.42 ± 3.85 |

**Table 4.** SHADOZ QR median (50%-ile) annual ozone trends values (1998-2023) for TrCO (surface to tropopause) and FTp (700-300 hPa) columns in DU/decade and in %/decade with ±2*sigma. Trends

| SHADOZ QR 1998-2023 L1 Annual Ozone Trends | | | | | | | |
|---|---|---|---|---|---|---|---|
| **Station** | **Latitude** | **Longitude** | **L1 Obs #** | **TrCO (surf-Tp) Trend ± 2*sigma (DU/decade)** | **TrCO (surf-Tp) Trend ± 2*sigma (%/decade)** | **FTp (300-700 hPa) Trend ± 2*sigma (DU/decade)** | **FTp (300-700 hPa) Trend ± 2*sigma (%/decade)** |
| **Samoa** | -14.23 | -170.56 | 797 | -0.29 ± 0.54 | -1.41 ± 2.59 | -0.04 ±0.36 | -0.44 ± 3.58 |
| *Hilo* | *19.43* | *-155.04* | *1142* | *-0.71 ± 0.72* | *-2.21 ± 2.25* | *-0.20 ± 0.24* | *-1.33 ± 1.51* |
| **San Cristobal** | -0.89 | -89.61 | 350 | -0.44 ± 1.14 | -1.69 ± 4.42 | -0.03 ±0.48 | -0.24 ± 3.79 |
| **Paramaribo** | 5.80 | -55.21 | 855 | 0.22 ± 0.62 | 0.80 ± 2.27 | 0.09 ± 0.34 | 0.67 ± 2.62 |
| **Natal** | -5.42 | -35.38 | 676 | **1.04 ± 0.68** | **3.04 ± 2.00** | **0.56 ± 0.48** | **3.29 ± 2.79** |
| **Ascension Island** | -7.58 | -14.24 | 676 | 0.20 ± 0.84 | 0.53 ± 2.19 | 0.04 ± 0.40 | 0.21 ± 2.09 |
| *Irene* | *-25.90* | *28.22* | *387* | *0.53 ± 0.98* | *1.44 ± 2.63* | *0.38 ± 0.48* | *2.02 ± 2.63* |
| **Nairobi** | -1.27 | 36.80 | 872 | 0.26 ± 0.70 | 0.94 ± 2.53 | 0.16 ± 0.46 | 1.11 ± 3.13 |
| *Reunion* | *-21.06* | *55.48* | *735* | ***2.63 ± 0.78*** | ***7.22 ± 2.14*** | ***0.90 ± 0.40*** | ***5.22 ± 2.31*** |
| **Kuala Lumpur** | 2.73 | 101.27 | 456 | 0.67 ± 1.12 | 2.68 ± 3.69 | 0.10 ± 0.50 | 0.95 ± 4.77 |
| *Hanoi\** | *21.01* | *105.80* | *350* | *1.94 ± 2.18* | *4.85 ± 5.45* | *0.43 ± 0.96* | *2.46 ± 5.52* |
| **Watukosek** | -7.46 | 112.43 | 326 | 0.71 ± 1.74 | 2.87 ± 6.99 | 0.22 ± 0.78 | 2.07 ± 7.26 |
| **Fiji** | -18.13 | 178.40 | 391 | -0.28 ± 0.84 | -1.16 ± 3.54 | 0.17 ± 0.68 | 1.48 ± 5.71 |

\* Hanoi dataset starts in 2004 (not 1998).

**Table 5.** SHADOZ QR median (50%-ile) annual ozone trends values (1998-2023 and 2008-2019) for TrCO (surface to tropopause) columns in DU/decade with ±2*sigma. Trends with p-values <0.05 are

shown in bold. L1 data is daily data from the HEGIFTOM database
(https://hegiftom.meteo.be/datasets).

| SHADOZ QR L1 Annual TrCO Trends for 1998-2023 and 2008-2019 | | | | |
|---|---|---|---|---|
| Station | Latitude | Longitude | 1998-2023 TrCO (surf-Tp) Trend ± 2*sigma (DU/decade) | 2008-2019 TrCO (surf-Tp) Trend ± 2*sigma (DU/decade) |
| Samoa | -14.23 | -170.56 | -0.29 ± 0.54 | **-1.74 ± 1.70** |
| Hilo | 19.43 | -155.04 | **-0.71 ± 0.72** | **-1.46 ± 1.46** |
| San Cristobal | -0.89 | -89.61 | -0.44 ± 1.14 | -0.39 ± 2.42 |
| Paramaribo | 5.80 | -55.21 | 0.22 ± 0.62 | 0.47 ± 1.26 |
| Natal | -5.42 | -35.38 | **1.04 ± 0.68** | -1.06 ± 2.06 |
| Ascension Island | -7.58 | -14.24 | 0.20 ± 0.84 | 1.26 ± 2.04 |
| Irene | -25.90 | 28.22 | 0.53 ± 0.98 | -1.76 ± 2.74 |
| Nairobi | -1.27 | 36.80 | 0.26 ± 0.70 | 0.39 ± 1.58 |
| Reunion | -21.06 | 55.48 | **2.63 ± 0.78** | 1.67 ± 1.92 |
| Kuala Lumpur | 2.73 | 101.27 | 0.67 ± 1.12 | 0.90 ± 1.86 |
| Hanoi* | 21.01 | 105.80 | 1.94 ± 2.18 | 0.80 ± 1.80 |
| Watukosek | -7.46 | 112.43 | 0.71 ± 1.74 | 0.00 ± 2.28 |
| Fiji | -18.13 | 178.40 | -0.28 ± 0.84 | -1.58 ± 2.46 |

* Hanoi dataset starts in 2004 (not 1998).

**Table 6.** Summary of annual tropopspheric (FT, UT and TrCO) ozone trends values for the tropics in
ppbv/decade and %/decade with ±2*sigma (estimated in some cases where different units published)
from TOAR-II relevant papers separated into 5 regions: Equatorial Americas, Atlantic and West Africa,
East Africa, Southeast Asia and Samoa.  There are 6 different references, including this work,

1155 representing ground-based and satellite observations covering the 1995-2023 time period (time ranges
1156 do vary study to study).
1157

| Region | Reference | Data Description | Time Period | FT Trends** | | UT Trends** | | TrCO Trends** | |
|---|---|---|---|---|---|---|---|---|---|
| | | | | ppbv /decade[t] | % /decade | ppbv /decade[t] | % /decade | ppbv /decade[t] | % /decade |
| Equatorial Americas | This work | ozonesonde data from SHADOZ: San Cristobal and Paramaribo (5-10km for FT, 10-15km for UT, surface to tropopause for TrCO) | 1998-2023 | -0.6 ± 1.8 | -0.9 ± 3.7 | -2.1 ± 3.1 | -3.5 ± 4.5 | -0.5 ± 1.6 | -1.0 ± 3.3 |
| | | IAGOS and SHADOZ data for Equatorial Americas (700-300hPa for FT) | 1998-2023 | 0.00 ± 1.2 | -0.01 ± 2.6 | NA | NA | NA | NA |
| | | OMI/MLS[$] tropospheric column (surface to tropopause) | 2005-2023 | NA | NA | NA | NA | 1.4 ± 1.1 | 3.1 ± 2.5 |
| | Gaudel et al (2024) | Fused IAGOS + SHADOZ (FT from Figure S24 and TrOC from Table 1) | 2004–2019 | -1.5 ± 0.75 | -3.3 ± 1.7 | NA | NA | -1.3 ± 0.4 | -2.9 ± 0.9 |
| | Froidevaux et al (2025) | Aura MLS UT data averaged over 147 and 215 hPa based on Figure 5 and Table S1 | 2005–2020 | NA | NA | 2.0 ± 1.3 | 4.0 ± 2.7 | NA | NA |
| | Van Malderen et al (2025a) | HEGIFTOM* Paramaribo ozonesonde data (700-300 hPa for FT) from Table 2 | 2000-2022 | 0.3 ± 1.1 | 0.7 ± 3.0 | NA | NA | NA | NA |
| | Boynard et al (2025) | Climate Data Record (CDR) from IASI for TrCO (surface to thermal tropopause) based on Figures 12 & 13 | 2008-2023 | NA | NA | NA | NA | -1.8 ± 0.5 | -4.0 ± 1.1 |
| Atlantic and West Africa | This work | ozonesonde data from SHADOZ: Natal and Ascension (vertical columns same as above) | 1998-2023 | 1.2 ± 1.8 | 1.9 ± 2.2 | 2.1 ± 2.1 | 3.4 ± 2.9 | 1.3 ± 1.1 | 1.9 ± 1.8 |
| | | IAGOS and SHADOZ data for Atlantic and West Africa | 1998-2023 | 0.5 ± 1.5 | 0.7 ± 2.3 | NA | NA | NA | NA |

| Region | Reference | Description | Period | | | | | | |
|---|---|---|---|---|---|---|---|---|---|
| | | (700-300hPa for FT) | | | | | | | |
| | | OMI/MLS$ tropospheric column (surface to tropopause) | 2005-2023 | NA | NA | NA | NA | 0.7 ± 0.9 | 1.3 ± 1.4 |
| | **Gaudel et al (2024)** | Natal/Ascension (SHADOZ only) and West Africa (IAGOS only); FT from Figure S24 and TrOC from Table 1 | 2004–2019 | NA<br>-0.7 ± 1.5 | NA<br>-1.3 ± 2.8 | NA | NA | -0.6 ± 0.5<br>0.4 ± 1.0 | -1.1 ± 0.9<br>0.7 ± 1.8 |
| | **Froidevaux et al (2025)** | same as above | 2005–2020 | NA | NA | 1.9 ± 1.3 | 3.7 ± 2.7 | NA | NA |
| | **Van Malderen et al (2025a;2025b)** | HEGIFTOM* Ascension/Natal ozonesonde data from Table 2 (ref a) and merged Gulf of Guinea data (700-300 hPa for FT) Table S3 (ref b) | 2000-2022<br>1995-2022 | 0.0 ± 1.5<br>-0.5 ± 0.7 | 0.0 ± 2.7<br>-1.0 ± 1.3 | | | | |
| | **Boynard et al (2025)** | CDR from IASI/Metop for TRCO (surface to thermal tropopause) based on Figures 12 & 13 | 2008-2023 | NA | NA | NA | NA | -2.7 ± 0.5 | -4.9 ± 2.0 |
| **East Africa** | **This work** | ozonesonde data from SHADOZ: Nairobi (vertical columns same as above) | 1998-2023 | 0.6 ± 1.8 | 0.5 ± 3.0 | -1.0 ± 2.1 | -1.5 ± 3.2 | 0.5 ± 1.3 | 1.1 ± 2.5 |
| | | IAGOS and SHADOZ data for East Africa (700-300hPa for FT) | 1998-2023 | 0.5 ± 1.5 | 0.8 ± 2.7 | NA | NA | NA | NA |
| | | OMI/MLS$ tropospheric column (surface to tropopause) | 2005-2023 | NA | NA | NA | NA | 0.2 ± 2.0 | 0.6 ± 4.5 |
| | **Gaudel et al (2024)** | NA | NA | NA | NA | NA | NA | NA | NA |
| | **Froidevaux et al (2025)** | same as above | 2005–2020 | NA | NA | 1.8 ± 1.3 | 3.7 ± 2.7 | NA | NA |
| | **Van Malderen et al (2025a)** | HEGIFTOM* Nairobi ozonesonde data (700-300 hPa for FT) from Table 2 | 2000-2022 | 0.3 ± 1.5 | 0.7 ± 3.4 | NA | NA | NA | NA |
| | **Boynard et al (2025)** | CDR from IASI/Metop for TRCO (surface to thermal | 2008-2023 | NA | NA | NA | NA | -1.8 ± 0.5 | -3.6 ± 1.0 |

| Region | Reference | Description | Years | | | | | | |
|---|---|---|---|---|---|---|---|---|---|
| | | tropopause) based on Figures 12 & 13 | | | | | | | |
| | **This work** | ozonesonde data from SHADOZ: Kuala Lumpur and Watukosek (vertical columns same as above) | 1998-2023 | 0.6 ± 1.2 | 1.0 ± 2.5 | 0.0 ± 1.0 | 1.3 ± 3.6 | 1.1 ± 1.1 | 2.6 ± 2.3 |
| | | IAGOS and SHADOZ data for Equatorial Southeast Asia (700-300hPa for FT) | 1998-2023 | 0.6 ± 1.3 | 1.6 ± 3.2 | NA | NA | NA | NA |
| | | OMI/MLS$ tropospheric column (surface to tropopause) | 2005-2023 | NA | NA | NA | NA | 2.0 ± 2.2 | 5.6 ± 6.0 |
| | **Gaudel et al (2024)** | Fused IAGOS + SHADOZ for SE Asia and Malaysia/Indonesia ; FT from Figure S24 and TrOC from Table 1 | 2004–2019 | 3.0 ± 1.5 1.5 ± 1.5 | 6.7 ± 3.3 5.0 ± 5.0 | NA | NA | 2.8 ± 1.4 3.4 ± 1.3 | 5.6 ± 2.8 8.5 ± 3.2 |
| **Southeast Asia** | **Stauffer et al (2024)** | ozonesonde data from SHADOZ: Kuala Lumpur and Watukosek (5-10km for FT, 10-15km for UT, surface to tropopause for TrCO) | 1998-2022 | 0.5 ±1.0 | 1.3 ± 2.7 | 0.0 ± 1.0 | 1.3 ± 2.7 | 1.3 ± 1.0 | 3.4 ± 2.6 |
| | **Froidevaux et al (2025)** | same as above | 2005–2020 | NA | NA | 2.2 ± 1.6 (up to 8.0) | 4.0 ± 2.8 (up to 14) | NA | NA |
| | **Van Malderen et al (2025a;2025b)** | HEGIFTOM* Kuala Lumpur alone from Table 2 (ref a) and merged SE Asia/ Malaysia data (700-300 hPa for FT) from Table S3 (ref b) | 2000-2022 1995-2022 | 0.8 ± 1.1 3.1 ± 1.1 | 2.2 ± 3.0 6.2 ± 2.2 | NA | NA | NA | NA |
| | **Boynard et al (2025)** | CDR from IASI/Metop for TRCO (surface to thermal tropopause) based on Figures 12 &13 | 2008-2023 | NA | NA | NA | NA | 0.0 ± 0.5 | 0.0 ± 1.4 |
| **Samoa** | **This work** | ozonesonde data from SHADOZ: Samoa (vertical columns same as above) | 1998-2023 | 0.6 ± 1.8 | 0.8 ± 4.4 | 0.0 ± 4.1 | -1.3 ± 9.2 | -0.5 ± 1.8 | -1.4±4.8 |

| | | | | | | | | |
|---|---|---|---|---|---|---|---|---|
| | IAGOS and SHADOZ data for Samoa (700-300hPa for FT) | 1998-2023 | -0.15 ± 1.5 | -0.4 ± 3.8 | NA | NA | NA | NA |
| | OMI/MLS[$] tropospheric column (surface to tropopause) | 2005-2023 | NA | NA | NA | NA | 2.5 ± 2.3 | 9.1 ± 8.3 |
| **Gaudel et al (2024)** | Samoa (SHADOZ only) ;TrOC from Table 1 | 2004–2019 | NA | NA | NA | NA | -1.1 ± 1.9 | -3.1 ± 5.4 |
| **Froidevaux et al (2025)** | same as above | 2005–2020 | NA | NA | 1.9 ± 1.5 | 3.4 ± 2.6 | NA | NA |
| **Van Malderen et al (2025a)** | HEGIFTOM* Samoa ozonesonde data (700-300 hPa for FT) from Table 2 | 2000-2022 | -0.07 ± 1.3 | -0.2 ± 4.2 | NA | NA | NA | NA |
| **Boynard et al (2025)** | CDR from IASI/Metop for TRCO (surface to thermal tropopause) based on Figures 12 & 13 | 2008-2023 | NA | NA | NA | NA | -2.7 ± 0.5 | -9.0 ± 1.7 |

1158
1159
1160 * Note HEGIFTOM data can be from the following ground networks: IAGOS, ozonesondes, FTIR, Umkehr,
1161 and Lidar.

1162
1163 ** Annual average trend plus 2*sigma.

1164
1165 [t] SHADOZ Trends have been converted from DU/decade to ppbv/decade for each layer so these are
1166 approximates values based on Tables 1 and 2.

1167
1168 [$] OMI/MLS trend values are from the 5x5 deg box that contains the SHADOZ station. In the cases where
1169 there are two SHADOZ stations (Nat/Asc, KL/Java, SC/Para), it's the average of the two OMI/MLS trends
1170 and confidence interval values.
1171

1172
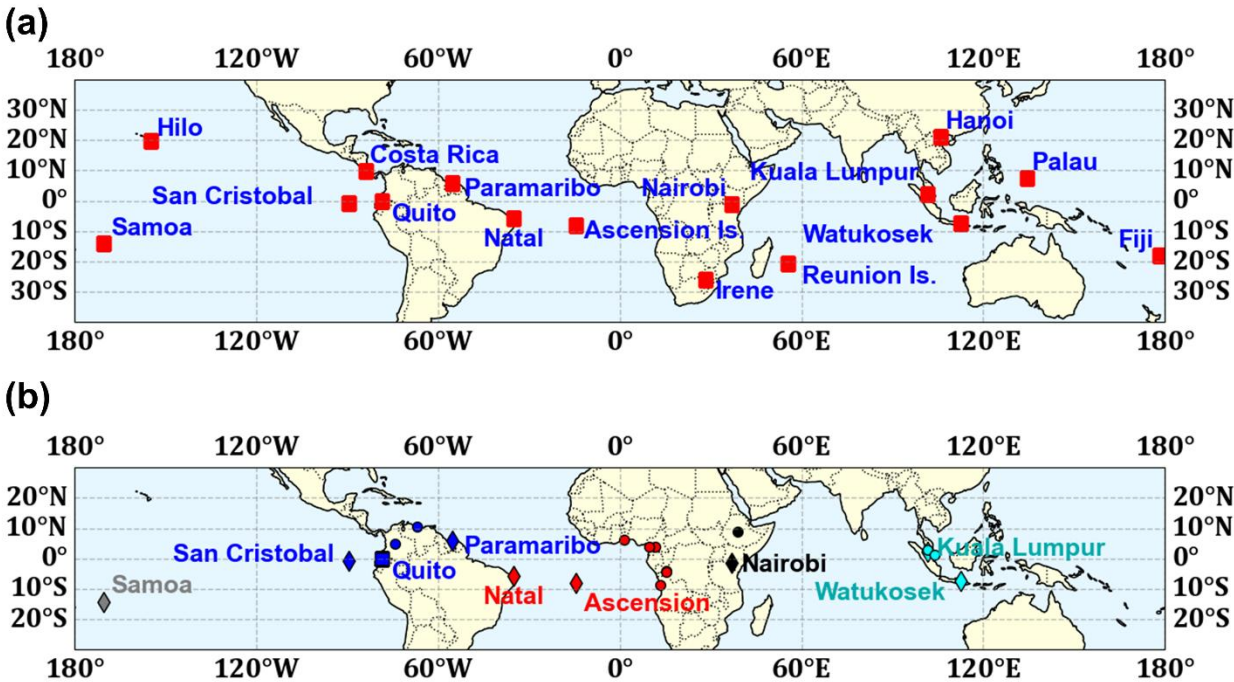


1173
1174
**Figure 1.** (a) Map of all SHADOZ stations in 2025 when the Quito and Palau records, that began in 2014 and 2015, respectively, joined the network. (b) SHADOZ sites used in T21 for 1998-2019 equatorial trends and here for 1998-2023 trends are represented with diamonds. SHADOZ stations whose combined records are examined within regions are colored blue for Equatorial Americas, red for Atlantic and cyan for equatorial southeast Asia. The airport locations from IAGOS include are those indicated with circles: red for Atlantic and West Africa, black for East Africa, cyan for the equatorial Southeast Asia region. For T21 and the trends here, the fifth station, including the combined stations, is Samoa (in gray). Quito (blue square) data are included in the Equatorial Americas trends. All station and airport locations are in **Table 1.** The 5 SHADOZ sites (2 individual and 3 combined) from T21 and for which trends are updated here appear in **Table 2** with the MLR trends. Individual SHADOZ and IAGOS site names within each region and their trends are shown in **Table 3**. Trends computed by QR for total column and FT ozone at 13 individual SHADOZ stations are summarized in **Table 4**.

1187
1188
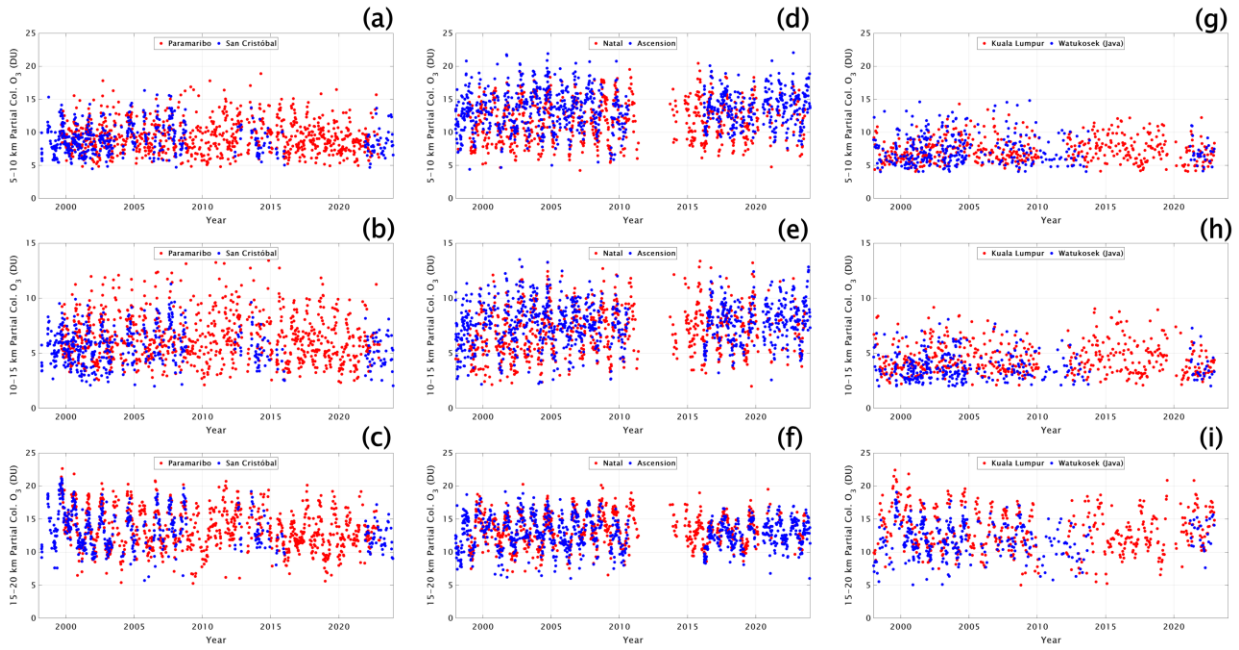
1189
1190
1191 **Figure 2.** Time-series of ozone column segments (in DU) for the combined SHADOZ stations, for the
1192 layers 5-10 km, 10-15 km, 15-20 km for: San Cristóbal-Paramaribo (a-c); Natal-Ascension (d-f); Kuala
1193 Lumpur-Watukosek (Java) (g-i). Station coordinates in **Table 1.**
1194
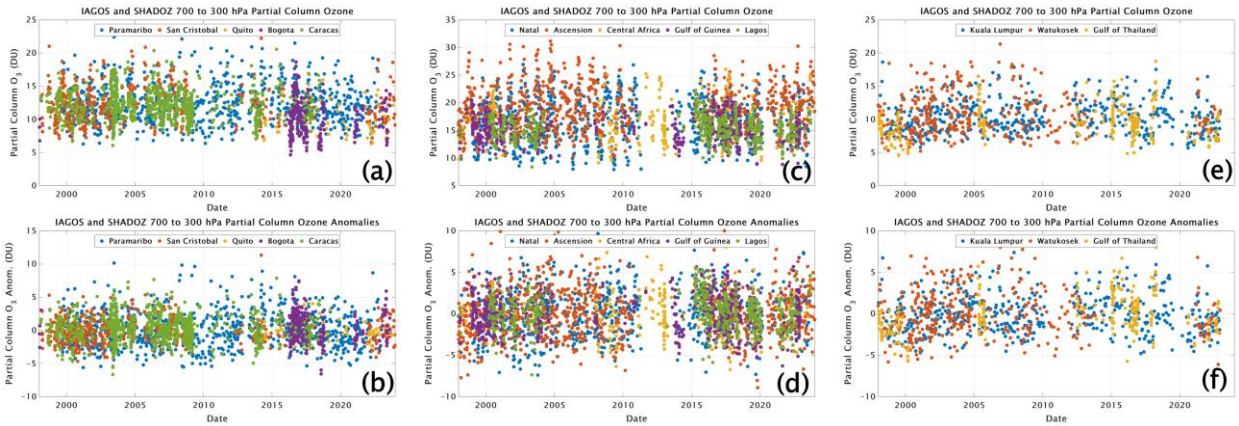


1195
1196
1197 **Figure 3.** Time-series of SHADOZ and IAGOS partial ozone column amounts and partial ozone column
1198 anomalies (in DU) for the pressure-defined mid-free troposphere, FTp (700 to 300 hPa), for (a-b)
1199 Equatorial Americas, (c-d) Atlantic and West Africa, and (e-f) Equatorial SE Asia.  The listing of the
1200 individual sites included in these datasets appears in **Table 3**.  Coordinates are in **Table 1.**
1201
1202

40
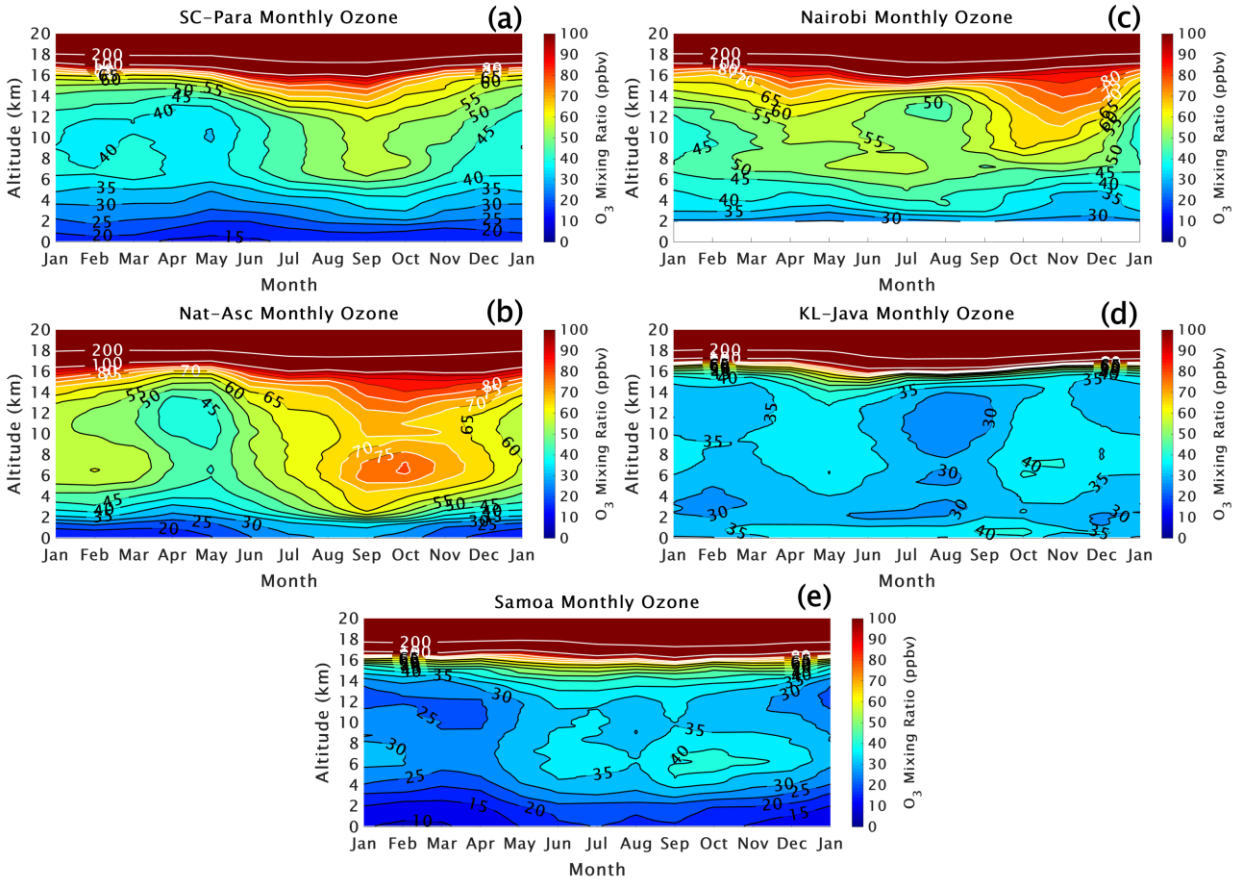
1203
**Figure 4.** Monthly averaged ozone mixing ratios from the surface to 20 km altitude for the five SHADOZ sites: (a) San Cristóbal – Paramaribo, (b) Natal – Ascension Island, (c) Nairobi, (d) Kuala Lumpur – Watukosek (Java), and (e) Samoa. Colors with black and white contour lines are shown for the ozone mixing ratios in ppbv.
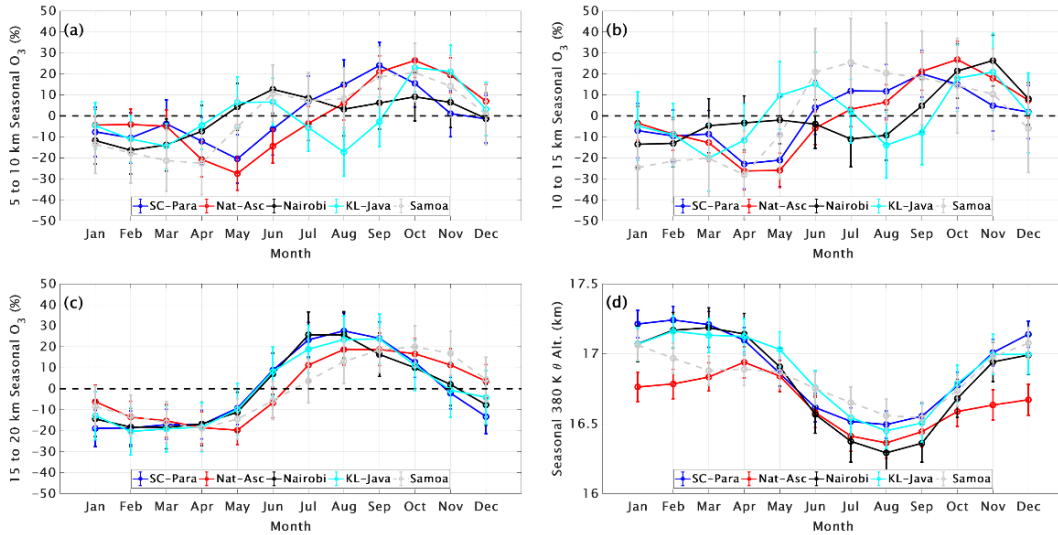


1207
**Figure 5**. Monthly ozone variability for the five T21 SHADOZ profiles, expressed as percent anomaly from annual mean, determined from the MLR model in the lower and middle FT (5-10 km: a, 10-15 km: b) and for the LMS (15-20 km: c). The tropopause Height (TH) seasonal cycle (d, in km) is based on the 380 K potential temperature surface from the radiosondes. Dots indicate monthly values; error bars display the 95% confidence intervals.

1212
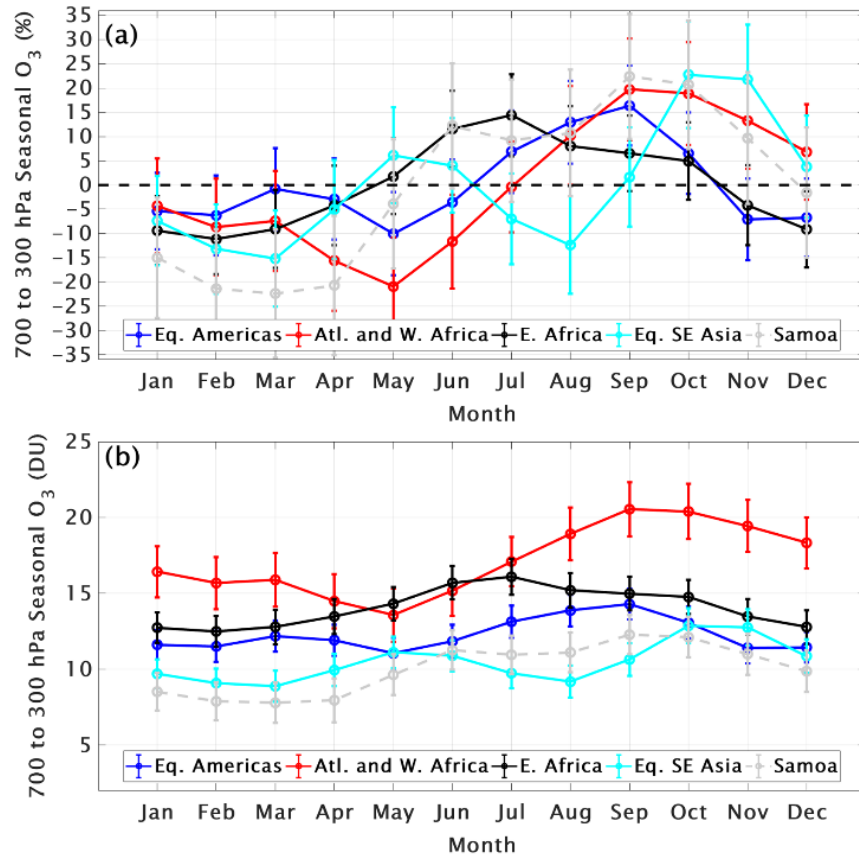
1213
1214
**Figure 6.** Monthly ozone variability for the five combined SHADOZ+IAGOS regions (defined in **Figure 1** and **Table 3**), expressed as anomaly from annual mean in (a) percent with actual values in DU (b), for FTp (700-300 hPa) column. Dots indicate the monthly values; error bars display the 95% confidence intervals.
1215
1216
1217
1218
1219
1220
1221
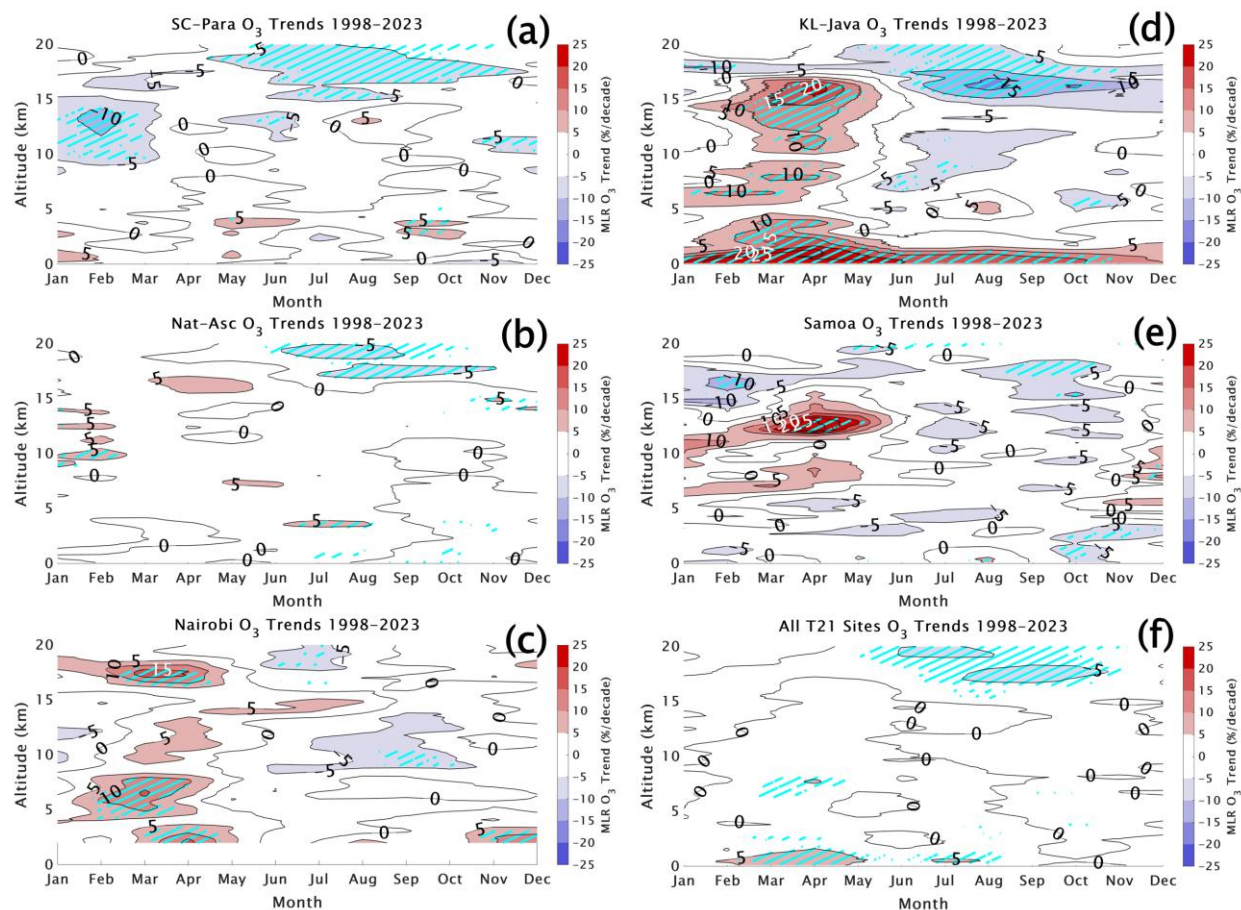
**Figure 7.** Monthly MLR ozone linear trends from 0 to 20 km in percent per decade for the SHADOZ T21 stations (a) San Cristóbal-Paramaribo (SC-Para); (b) Natal-Ascension (Nat-Asc) (c) Nairobi, (d) Kuala Lumpur-Watukosek (KL-Java); (e) Samoa. This is an update to Figure 6 in T21. In (f), average trends over (a) through (e) are displayed by combining the records from all eight individual T21 SHADOZ stations. Positive trends are shown in red shades and negative trends are shown in blue shades. Trends with p-values <0.05 (exceeding the 95% confidence interval) are shown with cyan hatching.

1231
1232
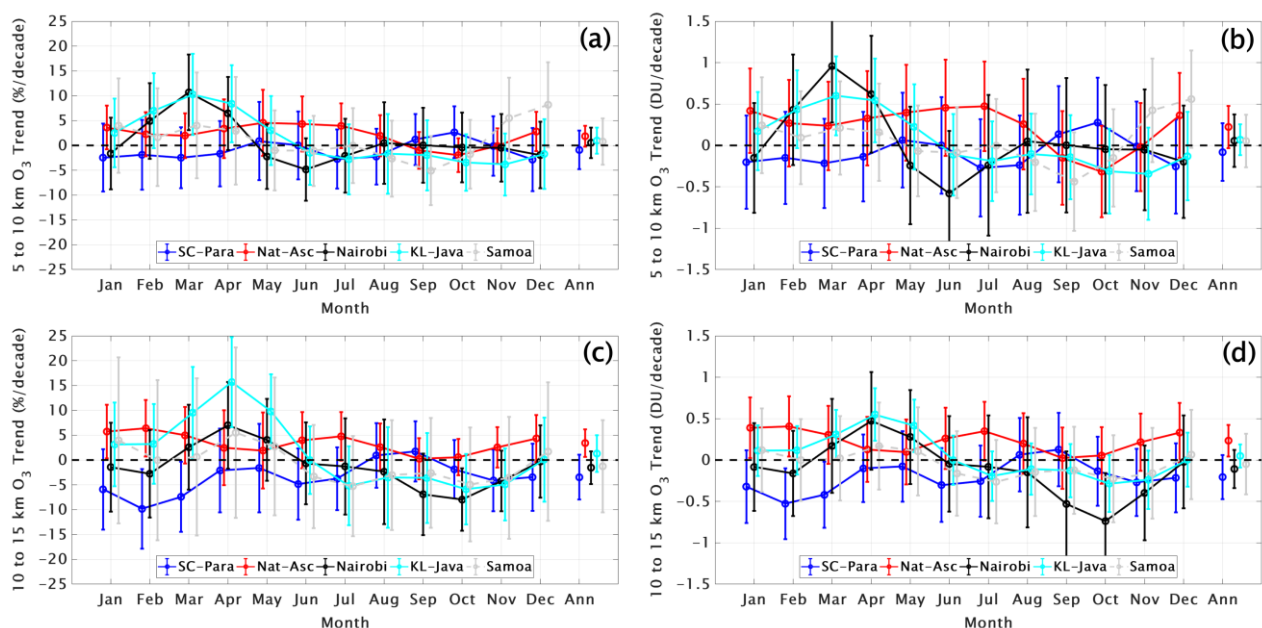


1233
1234 **Figure 8.** Monthly and annual MLR trends for five T21 SHADOZ sites in lower FT ozone column,
1235 integrated from 5-10 km, for (a) %/decade (b) DU/decade; (c) and (d) same as (a) and (b)
1236 respectively but for upper FT ozone column (10-15 km), derived from SHADOZ sondes. Dots
1237 indicate the monthly and annual trends; error bars display the 95% confidence intervals.
1238
1239
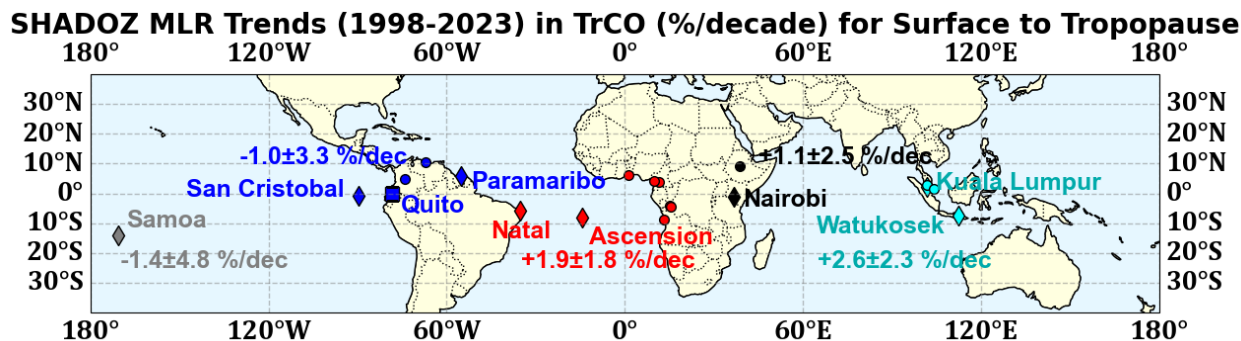


1240
1241
1242 **Figure 9.** Summary map of the annual 1998-2023 MLR trends for five T21 SHADOZ sites for the total
1243 tropospheric column ozone (TrCO), surface to tropopause, in %/decade from **Table 2** including the 95%
1244 confidence intervals.

**15–20 km Partial Column O$_3$ Trends**

**380 K $\theta$ Altitude Trends**

**TH to TH + 5 km Partial Column O$_3$ Trends**
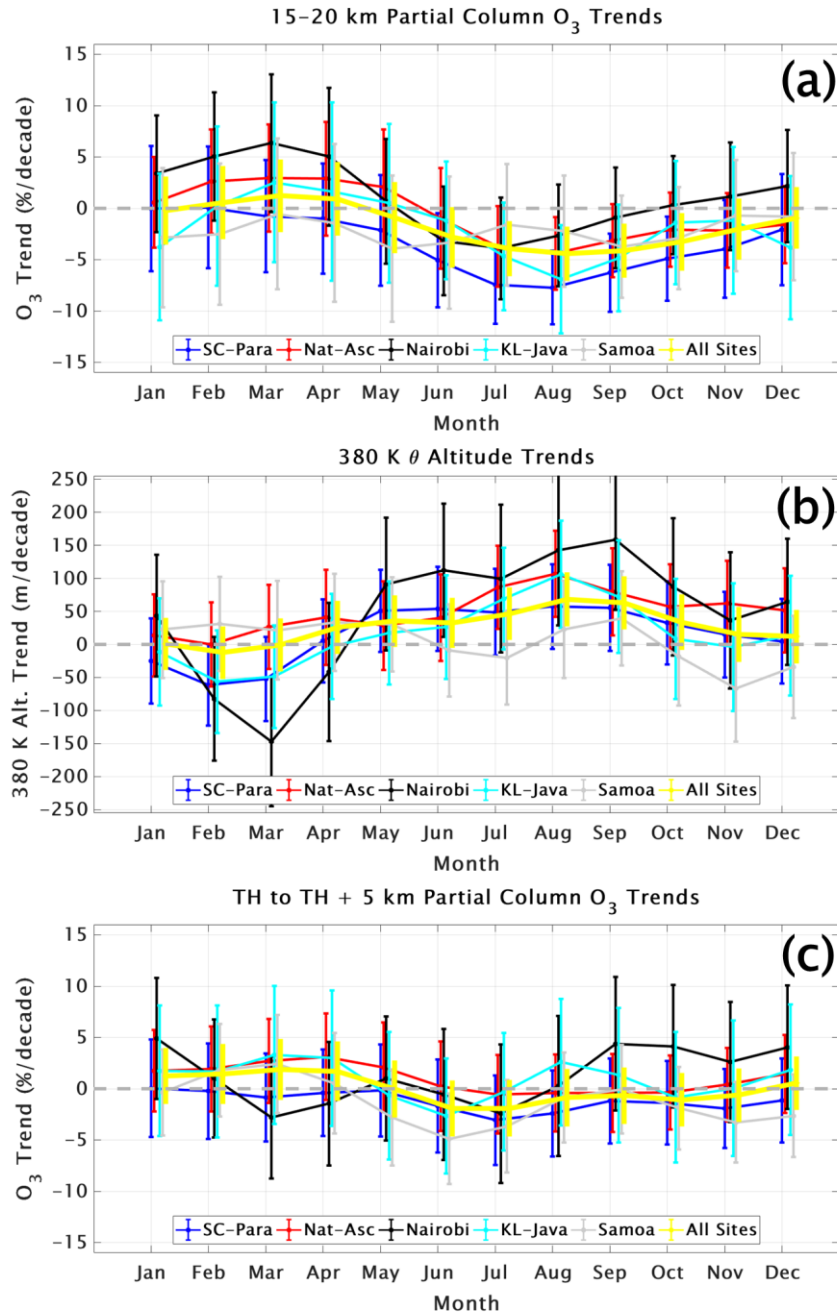
1245
1246 **Figure 10**. (a) Monthly MLR trends (colored dots) derived from SHADOZ T21 stations
1247 highlighting a July-October decrease in LMS ozone in 15-20km layer; yellow dots denote the
1248 mean of all T21 stations, with error bars indicating the 95% confidence intervals. (b)
1249 Corresponding TH trends (380 K potential temperature; θ) derived from the radiosondes. (c)
1250 Same as (a) except trends have been computed for the segments between the tropopause and 5
1251 km above the TH. Compared to (a) the trends in the tropopause referenced ozone column (c)
1252 become close to zero throughout the year.
1253
1254
1255
1256
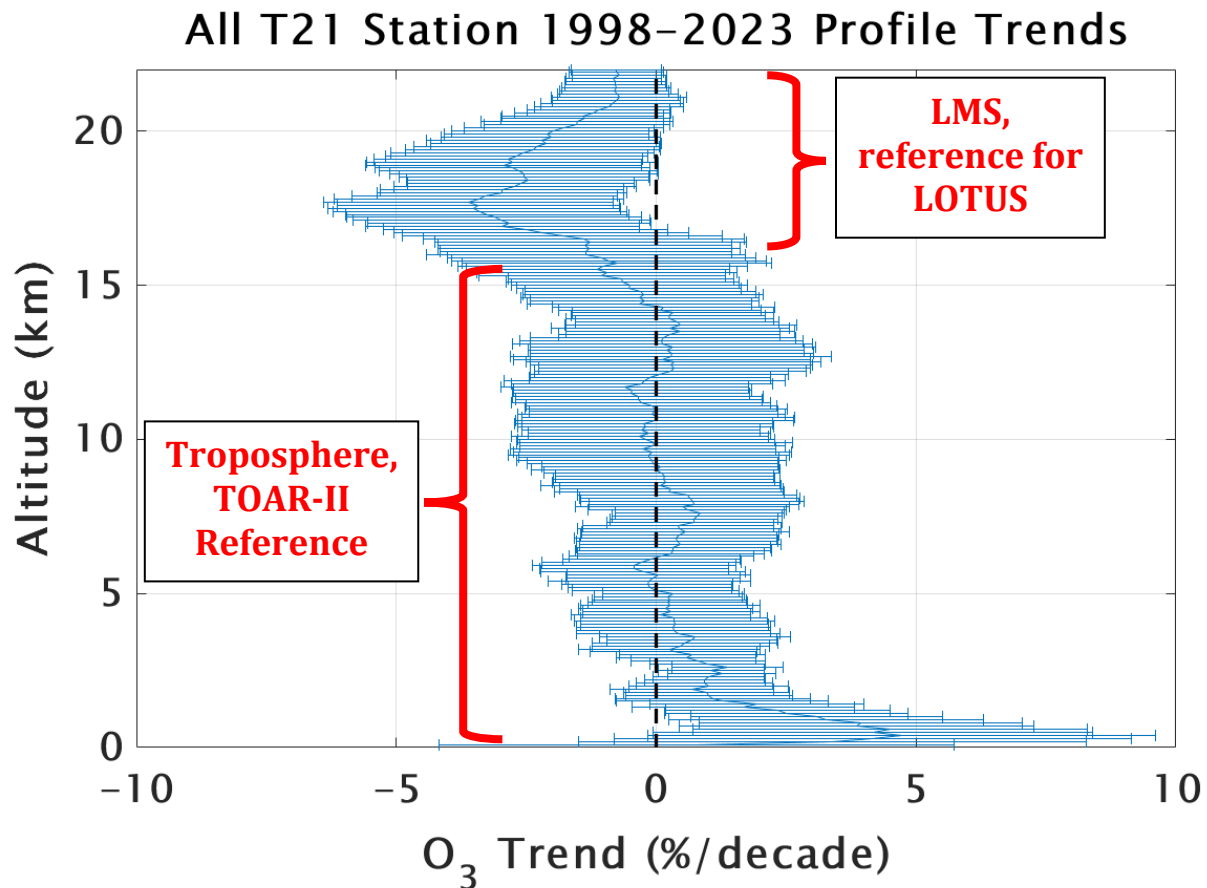
**Figure 11.** The total mean annual ozone trend (solid blue line), based on mixing ratio changes in 100-m intervals, from the surface to 22 km for all eight T21 SHADOZ profile datasets in %/decade with the 95% confidence interval range denoted. The LMS region of interest to the stratospheric community, e.g., the LOTUS activity, while the tropospheric segment is marked as the primary TOAR-II focus. The -4%/decade trend in LMS ozone is similar to that derived from satellites in that region. The mean change throughout the FT is negligible and within the uncertainty range except below 2 km where mean increases ~+5%/decade are indicated. The near-surface trends are primarily a result of rapid increases in urbanized regions of equatorial SE Asia (Stauffer et al., 2024).

1267 (a)



1268 **(b)**



1269
1270

1271   **(c)**



1272
1273   **(d)**
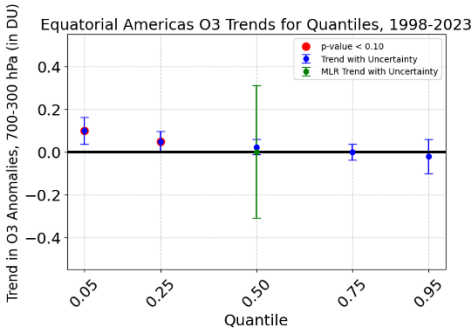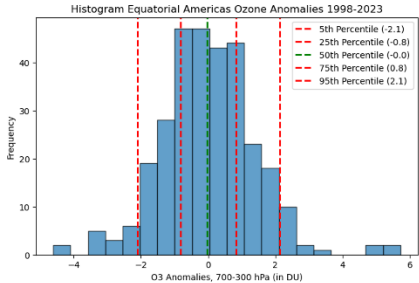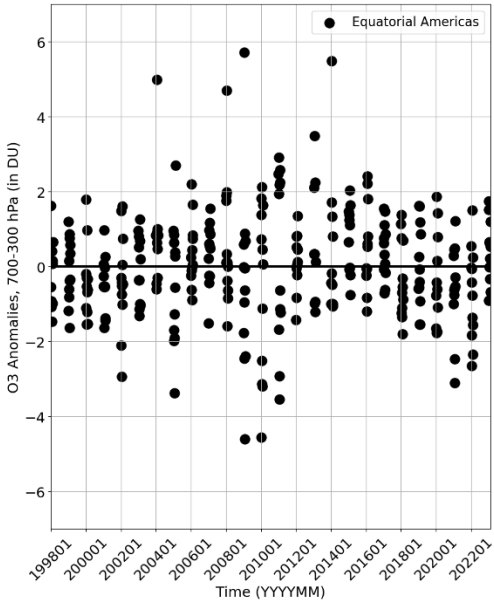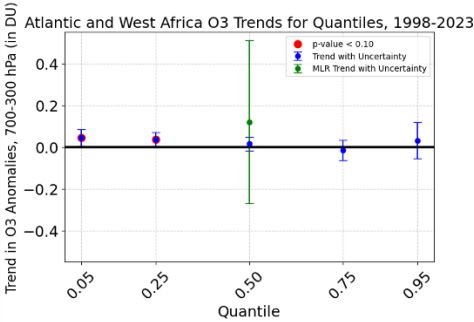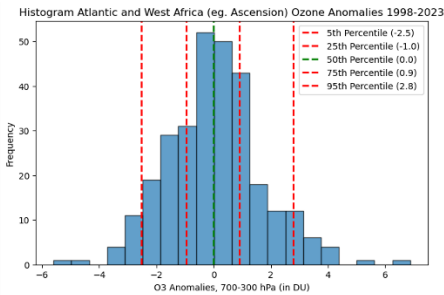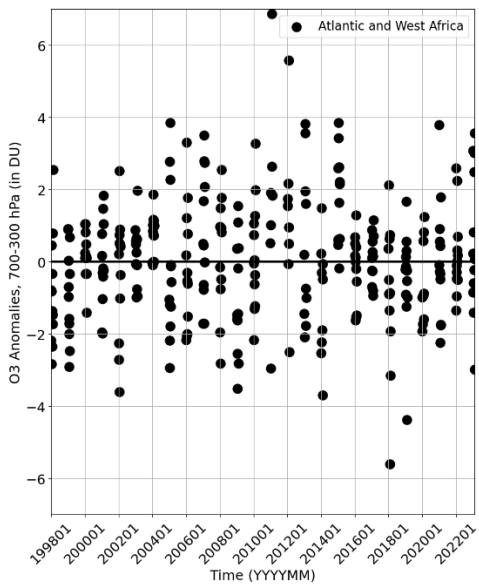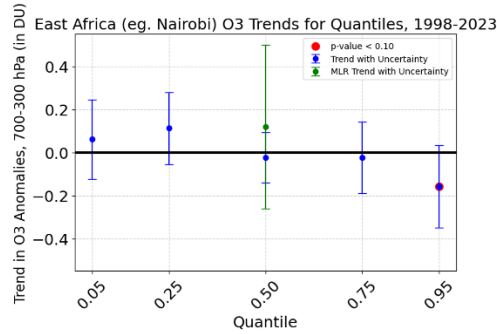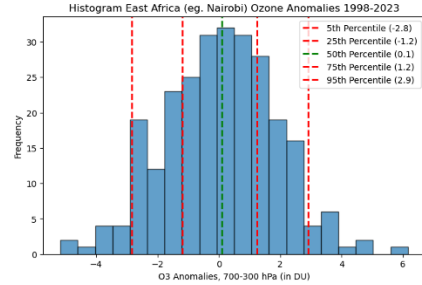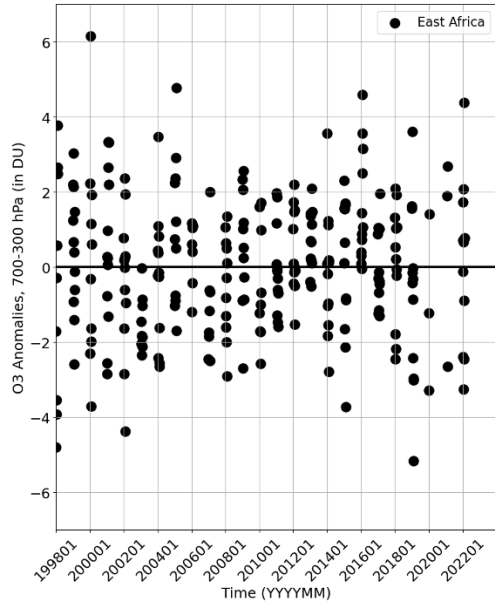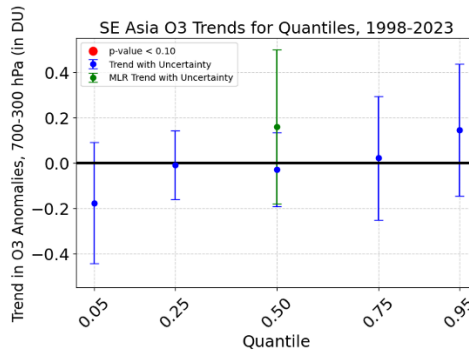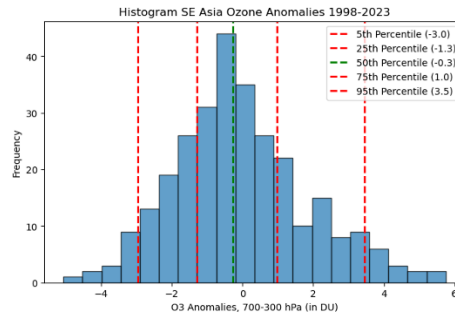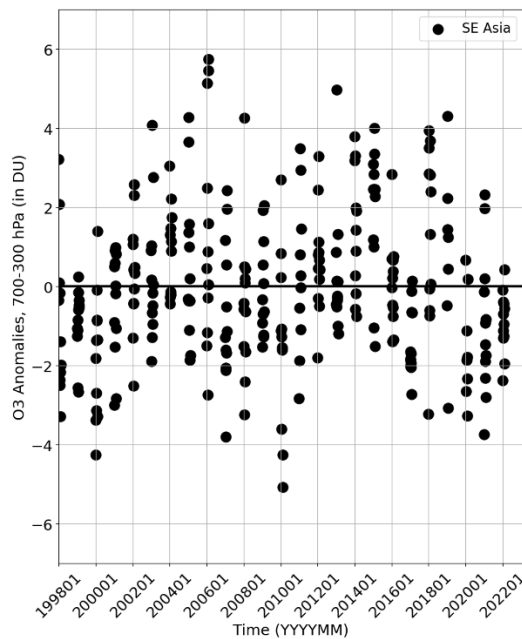


1274
1275
1276
1277   **Figure 12.** FTp column ozone segment anomalies (monthly means) from SHADOZ sondes and IAGOS data, as
1278   described in **Table 3.** Each frame displays the anomalies timeseries in DU at the left, a histogram of those
1279   anomalies in DU (each has a unique scale, ozone anomaly values for each percentile (dashed lines) are in
1280   parentheses) and the trends distribution by quantiles. Trends from annual MLR ozone (median, 50%-ile) over
1281   1998-2023 are green circles with their respective +/- 2sigma bars. The same period trends computed with QR by
1282   quantiles (0.05= lowest 5%-ile), 0.25 (25%-ile), 0.50 for median trends, 0.75 (75%-ile) and 0.95 (95%-ile) are blue
1283   circles.  Red circles denote p<0.10.  (a) equatorial Americas; (b) Atlantic and West Africa region; (c) east Africa; (d)
1284   equatorial southeast Asia.
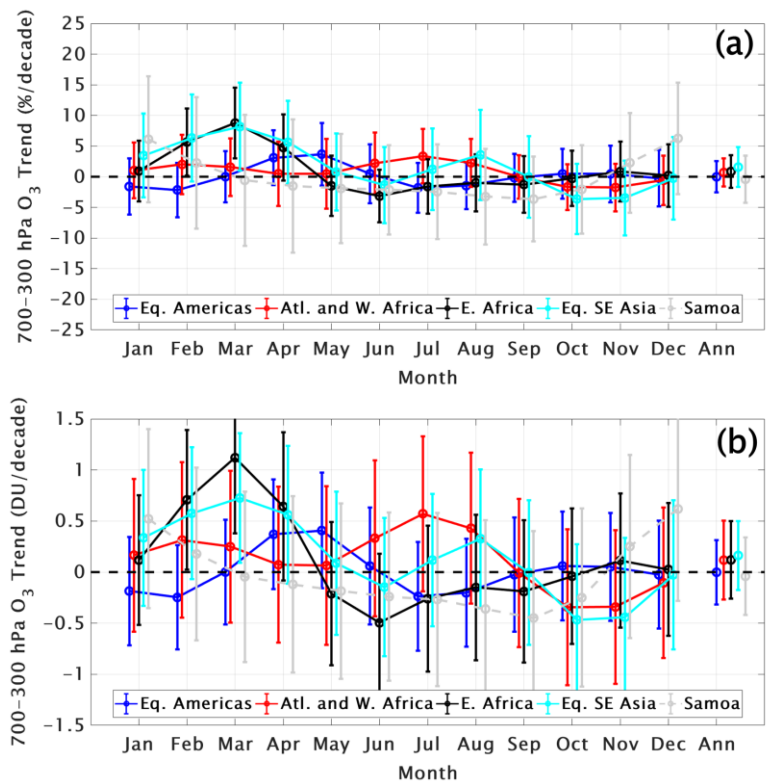
**Figure 13.** Monthly and annual MLR ozone trends for 5 combined SHADOZ+IAGOS regions, defined in **Table 3**, for FTp column in (a) %/decade and (b) DU/decade. Dots indicate the monthly and annual trends, whereas error bars display the 95% confidence intervals.
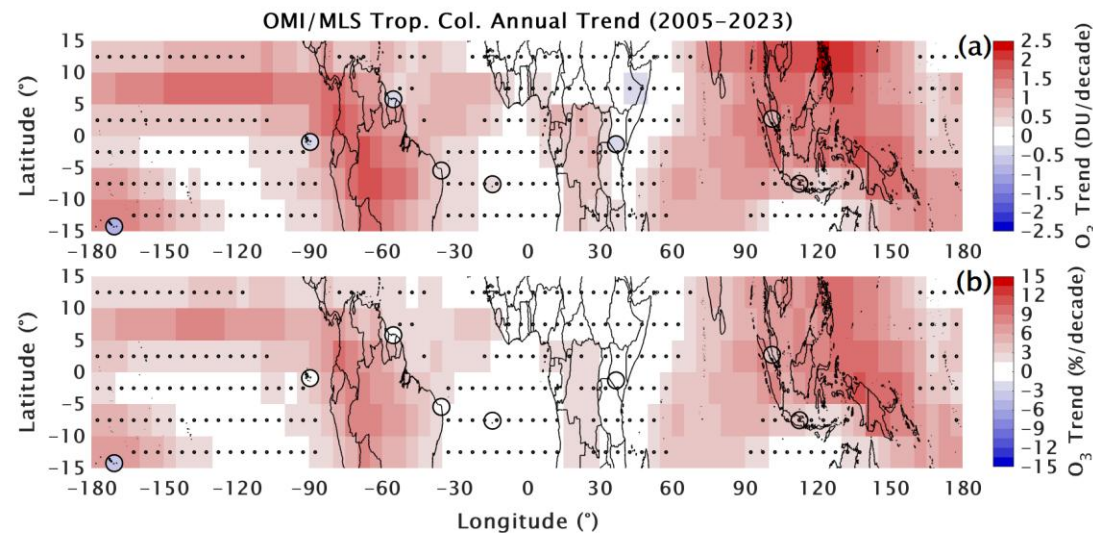


**Figure 14.** The most recent trends, 2005-2023, shown for the equatorial region based on updated OMI/MLS tropospheric total column ozone ($TrCO_{satellite}$) estimates in which a ~1% per decade positive drift in OMI was corrected. The corresponding SHADOZ-derived $TrCO_{sonde}$ column changes for 2005-2023 are superimposed on the map. Stippling indicates where OMI/MLS trends *do not* exceed the 95% confidence interval (i.e., historically referred to as statistically insignificant).
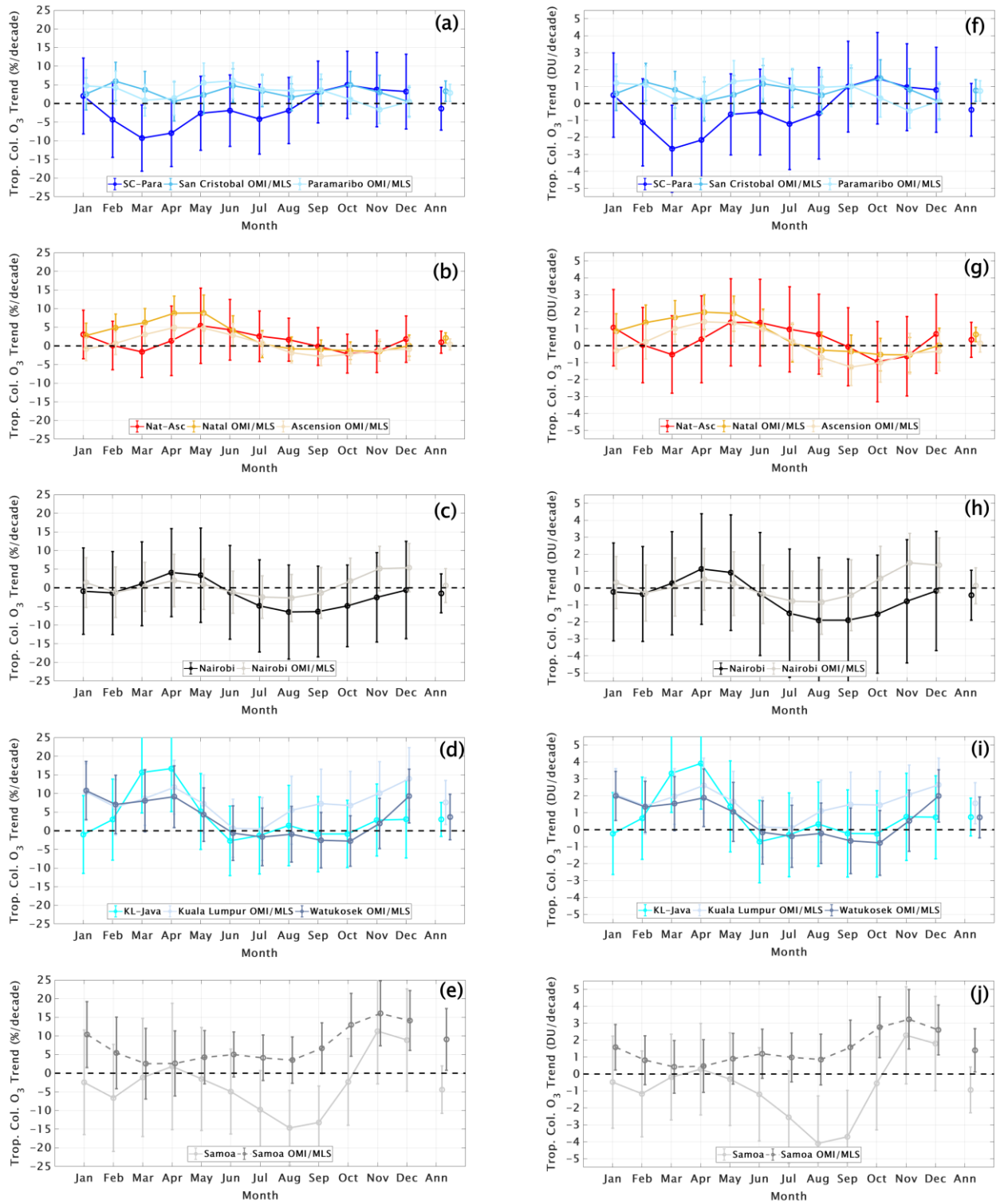
**Figure 15.** Monthly and annual MLR ozone trends in total tropospheric column (defined using the WMO lapse rate tropopause; TrCO) for the five T21 stations and the OMI/MLS pixel for each individual SHADOZ station each region. Dots indicate the ozone trend in % (a-e) and DU (f-j) per decade; error bars show the 95% confidence intervals.
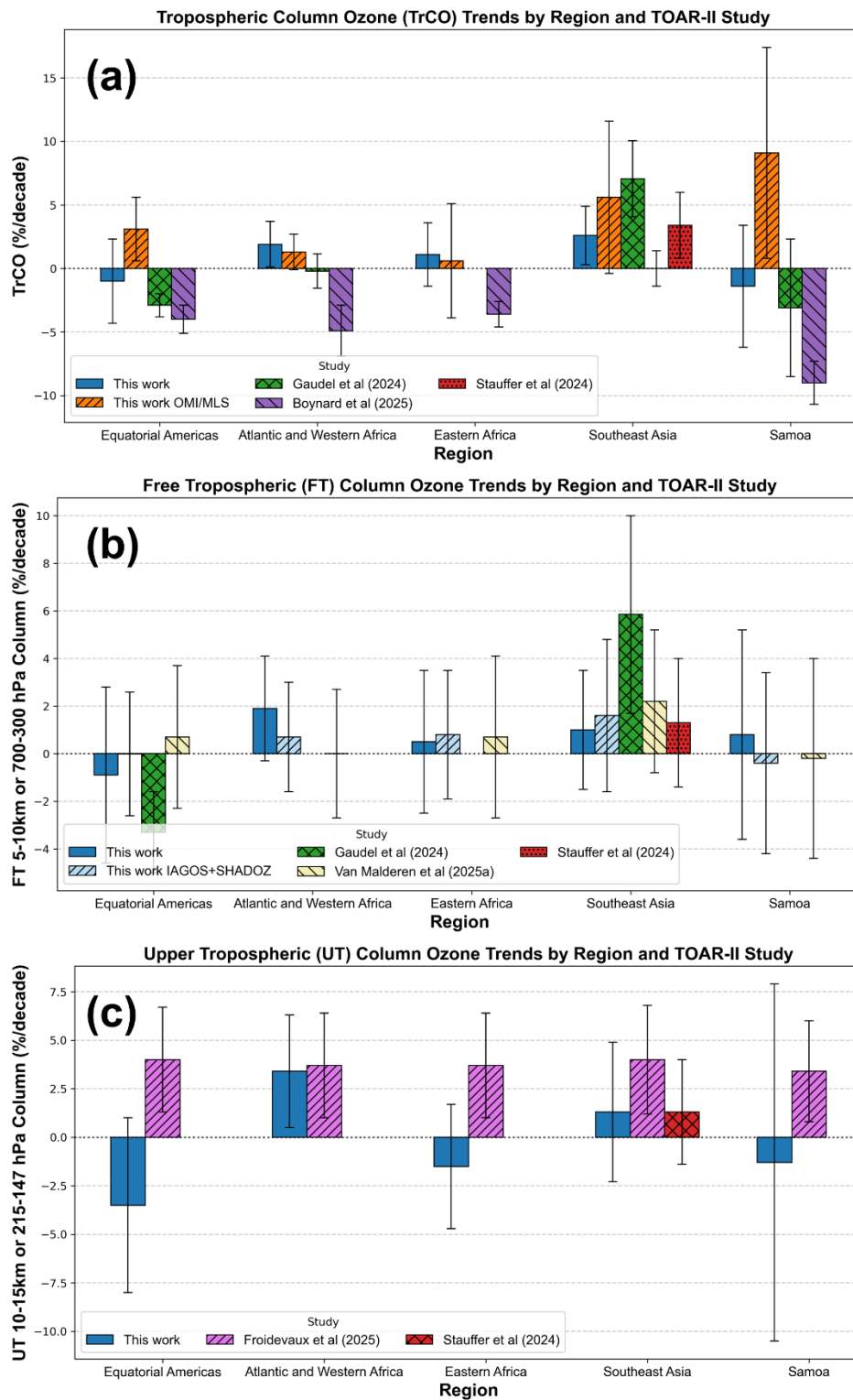
**Figure 16.** Summary of (a) TrCO, (b) FT, and (c) UT trends from multiple TOAR-II studies (detailed in Table 6). Trends are annual values in %/decade (sometimes estimated from each study); a different color represents each study across (a-c). Error bars show the 95% confidence intervals. If there are multiple values for a region in one study, a mean value is used.